Complete Assignments of Magnetic Resonances of Ribonuclease H from *Escherichia coli* by Double- and Triple-Resonance 2D and 3D NMR Spectroscopies

Toshio Yamazaki,[†,§] Mayumi Yoshida,[‖] and Kuniaki Nagayama*[,†,⊥]

Biometrology Lab, JEOL Ltd., Musashino, Akishima, Tokyo 196, Japan, and Tokyo Research Laboratories, Kyowa Hakko Kogyo Co. Ltd., Machida, Tokyo 194, Japan

Received December 10, 1992; Revised Manuscript Received March 19, 1993

ABSTRACT: Assignments of ^{1}H, ^{15}N, and ^{13}C magnetic resonances for ribonuclease H from *Escherichia coli* have been completed using double- and triple-resonance 2D and 3D NMR experiments. These assignments include all types of ^{1}H, ^{15}N, and ^{13}C nuclei detectable by NMR. The enzyme used, which cleaves the RNA moiety of an RNA–DNA duplex, consists of 155 amino acid residues and has 1962 nuclei (227 nitrogen, 762 carbons, and 973 protons) observable independently by NMR. Among those, 1868 nuclei (95%) have been assigned. Two methods, 3D HCH and ^{13}C–^{13}C–^{1}H heteroSQC/homoSQC, were newly devised to complete the side chain assignments. These methods were used to elucidate the $-CH_2-$ and –C–CH– substructures. Triple-resonance experiments to detect other types of substructures, (e.g., –N–CH– and –C–NH–) were also applied. In total, 10 kinds of 3D NMR experiments were used to complete the assignments. The chemical shifts obtained through the assignments were analyzed in terms of the tertiary structure of the protein molecule. Among the ^{13}C chemical shifts, larger secondary shifts (deviations from shifts at the random coil state) were observed for the C^{α}, C^{β}, and C′ nuclei, which reflect the local structures on the backbone, that is, the α-helix, β-sheet, and left-handed helix, respectively.

The recent development of the novel NMR techniques using multiple-dimensional NMR of isotopically enriched proteins allows us to assign the magnetic resonances of large proteins and to determine their tertiary structures. We have already reported a complete assignment for all of the backbone nuclei, except for carbonyl carbons, of RNase[1] H (Yamazaki et al., 1991). To study the mechanism of the enzymatic reaction in solution, it is important to investigate the structures and the electrostatic characters of the functional groups at atomic resolution. This kind of study primarily relies on the assignments of functional side chain groups. This report describes an extended study of NMR techniques to the complete assignments of all the NMR active half-spin nuclei including carboxyl, amino, and guanidino groups of proteins and the application to RNase H.

Ribonuclease H from *Escherichia coli* (155 amino acid residues, 17.6 kDa) is an enzyme with the specific function of cleaving the RNA moiety of an RNA–DNA hybrid duplex in the presence of Mg^{2+}, yielding a 3′-hydroxyl and a 5′-phosphate (Crouch, 1982). This enzyme cleaves only RNA–DNA hybrid duplexes, not single-strand RNAs, single-strand DNAs, DNA duplexes, or RNA duplexes. It has a weak specificity for the base sequence of the nucleic acids. This enzyme is also referred to as RNase H I because a second RNase H, RNase H II, was recently isolated from *E. coli* (Itaya, 1990).

From mutageneses (Kanaya et al., 1990) and X-ray crystallographic studies (Katayanagi et al., 1990; Yang et al., 1991), the residues D10, E48, and D70 have been found to be crucial for the hydrolysis and to be located at the crevice between the β-sheet and the α-helix II. Our previous study (Yamazaki et al., 1991) on the assignments of backbone magnetic resonances has shown that secondary structures, five β-strands forming a sheet and five α-helices, are formed in the solution state, which are similar to those seen in the X-ray structure. The same type of core structure was also suggested for the RNase H domain of the HIV reverse transcriptase in solution by NMR experiments (Powers et al., 1991b).

A complex structure of RNase H and an RNA–DNA duplex has been constructed from a substrate-free enzyme and an A form hybrid duplex (Nakamura et al., 1991). This model is derived on the basis of three experimental results, site-directed mutagenesis to vary K_m, binding energy calculations, and titration experiments using NMR measurements. The residues interacting with the substrate have been identified by titration of the RNA–DNA duplex monitored by changes in the chemical shifts of the nitrogen and hydrogen nuclei of the backbone amides (Yamazaki et al., 1991).

Divalent cation binding was also studied by X-ray (Katayanagi et al., 1991) and NMR experiments (Oda et al., 1991),

* To whom correspondence should be addressed.
† JEOL Ltd.
§ Present address: College of Arts and Sciences, The University of Tokyo, Komaba, Meguro-Ku, Tokyo 153, Japan.
‖ Kyowa Hakko Kogyo Co. Ltd
⊥ Present address: Biochemistry Research, The Hospital for Sick Children, 555 University Ave., Toronto, Ontario M5G 1X8, Canada.

[1] Abbreviations: Amino acid names are denoted by three-letter abbreviations. Residues from protein samples are denoted by a one-letter abbreviation of the amino acid followed by a residue number. Atoms are denoted by their atomic symbols followed by a position identifier (e.g., C^{α}). Backbone atoms are denoted as follows: N′, backbone amide nitrogen; C′, backbone carboxyl carbon; and H^{N}, backbone amide hydrogen. H^{x} indicates a proton attaching to C^{x}, N^{x}, O^{x}, or S^{x}. Atoms with attached protons are denoted as $C^{\alpha}H$. COSY, correlation spectroscopy; CT, constant time; DANTE, delays alternating with nutations for tailored excitation; HCACO, correlation spectroscopy for H^{α}–C^{α}–C′; HCCH, correlation spectroscopy for ^{1}H–^{13}C–^{13}C–^{1}H; HCH, correlation spectroscopy for ^{1}H–^{13}C–^{1}H; heteroSQC, =HSQC; HIV, human immunodeficiency virus; HMQC, heteronuclear multiple-quantum correlation spectroscopy; HNCA, correlation spectroscopy for H^{N}–N′–C^{α}; HNCO, correlation spectroscopy for H^{N}–N′–C′; HSQC, heteronuclear single-quantum correlation spectroscopy; MLEV, a pulse train for broad band heteronuclear decoupling; NOE, nuclear Overhauser effect; NOESY, nuclear Overhauser effect spectroscopy; homoSQC, homonuclear single-quantum correlation spectroscopy; RF, radio frequency; RNase, ribonuclease; TOCSY, total correlation spectroscopy.

0006-2960/93/0432-5656$04.00/0

which showed a single Mg^{2+} binds with a weak binding constant at residue D10 in the active site (K_d = 2 ~ 4 mM). A hydrolysis mechanism catalyzed by the three carboxylates and a magnesium ion has been also proposed, in which one carboxyl group is protonated and acts as a proton donor (Nakamura et al., 1991). Another mechanism with two divalent cations, which stabilize pentacovalent phosphorus intermediate, is also proposed (Yang et al., 1990). This study is intended to establish the NMR technique for assignments of functional groups, which are now focused for their significance in the mechanism of this enzyme.

2D NMR spectroscopy (Ernst et al., 1987), which reveals pairs of nuclei closely located through chemical bonds or through space in a molecule, has successfully been applied to the assignment of proton nuclei and the determination of the tertiary structures of proteins with molecular masses less than 10 kDa (Wüthrich, 1986). The limitation of molecular mass is brought about by degeneracy of chemical shifts of resonance frequencies. To overcome the problem of overlapping of resonance frequencies, multiple-dimensional NMR techniques have been devised, which started with the homonuclear method (Vuister et al., 1988; Oschkinat et al., 1988, 1989) and then was extended to the heteronuclear 3D experiments (Fesik & Zuiderweg, 1988; Marion et al., 1989a,b; Zuiderweg & Fesik, 1989).

The backbone nuclei of *E. coli* RNase H have been assigned by four kinds of heteronuclear 3D experiments, ^{13}C–^{1}H–^{1}H HMQC-NOESY, ^{13}C–^{1}H–^{1}H HMQC-TOCSY, ^{1}H–^{15}N–^{1}H NOESY-HMQC, and ^{1}H–^{15}N–^{1}H NOESY-HMQC, with the help of amino acid specific ^{15}N labelings (Nagayama et al., 1990; Yamazaki et al., 1991). The other methods have been developed to reveal chemical structures and to assign backbone nuclei, which made use of direct carbon–carbon and carbon–nitrogen couplings (Ikura et al., 1990; Kay et al., 1990a). In our study, these double- and triple-resonance techniques were also utilized to assign backbone carbonyl carbon nuclei.

Side chain proton nuclei are assigned with the COSY and TOCSY combination for small protein molecules. The NMR techniques specifically developed for the isotope spins have successfully extended the limit of molecular weight. Side chain carbon and nitrogen nuclei have been assigned with the use of uniform ^{13}C and ^{15}N enrichment (Oh et al., 1988; Oh & Markley, 1990). This idea is extended to 3D HCCH-COSY and 3D HCCH-TOCSY (Kay et al., 1990b; Bax et al., 1990a,b). In the 3D HCCH-COSY, ^{1}H magnetization is transferred through the attached and neighboring ^{13}C nuclei to the other ^{1}H nuclei and then detected. In the 3D HCCH-TOCSY, ^{1}H magnetization is transferred through multiple J couplings between ^{13}C nuclei. These methods have been shown to be powerful for assigning large parts of the side chain nuclei (Clore et al., 1990; Ikura et al., 1991; Pelton et al., 1991).

In the present study, almost all of the CH, CH_2, and CH_3 groups have been assigned by 3D HCCH-COSY and 3D HCCH-TOCSY. The nuclear spins of methylene groups usually have rapid transverse relaxation and hence give weak cross peaks in spectra even when this technique is used. Moreover, cross peaks often overlap each other. To identify pairs of hydrogen nuclei of methylene groups, a new technique called 3D HCH was developed, which allows for detection of methylene groups in the 3D spectral space spanned by two protons and one carbon chemical shifts.

Assignments given in this paper cover all proton, carbon, and nitrogen nuclei. Some of them are carbon and nitrogen nuclei that are not directly attached to protons. Enzymatic activities are often sustained with functional groups at the ends of side chains, which have no protons or which have rapidly exchanging protons. The assignment of nuclei at the side chain end groups is, therefore, quite important for understanding the molecular folding, molecular interactions, and catalytic activities. Negatively charged groups (carboxyl groups of Glu and Asp residues), positively charged groups (amino groups of Lys residues, guanidino groups of Arg residues, and imidazole rings of His residues), and amide groups of Asn and Gln residues have been assigned in this study.

Carbon nuclei at the γ position of aromatic residues have also been assigned, leading to unambiguous assignment of aromatic nuclei without the help of NOE connectivities. $C^{\delta 2}$ and $C^{\epsilon 2}$ nuclei of Trp residues have been assigned. For the assignment of these nuclei, 2D and 3D HSQC/HSQC experiments have been done, which include ^{1}H–^{15}N–^{13}C, ^{1}H–^{13}C–^{15}N, and ^{1}H–^{13}C–$^{13}C'$ variations. In the ^{1}H–^{13}C–$^{13}C'$ version, two carbons that have large differences between their chemical shifts are treated as heteronuclei (i.e., aliphatic carbons vs aromatic carbons or aliphatic carbons vs carbonyl carbons). When the two carbons have similar chemical shifts, a homonuclear version, heteroSQC/homoSQC, has been used.

EXPERIMENTAL PROCEDURES

As described in the previous report (Yamazaki et al., 1991), we prepared isotope-enriched protein samples from N4830 host cells and a plasmid containing ribonuclease H gene and λ-operator gene. This strain required His, Ile, and Val for growth, which brought about defects of enrichment of these residues. In this study, therefore, we used a new overproduction system. The plasmid vector pJAL600 contained structural gene *rnhA* under control of the bacteriophage λ promoters P_R and P_L, the λ-repressor gene cI^{ts857}, and the bacteriophage fd transcription terminator (Kanaya et al., 1992). The production level of the enzyme in *E. coli* HB101 holding pJAL600 was 40–50 mg/L, which was 3–4 times that used before.

An M9 minimum culture medium was used for isotope enrichments of protein samples. For ^{13}C enrichment, glucose uniformly and fully enriched with ^{13}C was used. For ^{15}N enrichment, ammonium chloride fully enriched with ^{15}N was used. The details of cultivation, induction, and purification were already reported (Yamazaki et al., 1991).

Three fully enriched protein samples were prepared. The first sample, which was uniformly enriched with ^{13}C, was used for the assignment of side chain nuclei in CH, CH_2, and CH_3 groups. The second sample, which was uniformly enriched with ^{15}N, was used for assignment of His ring nitrogen nuclei. The third sample, which was enriched both with ^{13}C and ^{15}N, was used to assign backbone carbonyl carbon and Pro nitrogen and aliphatic side chain nitrogen nuclei. In principle, a sample fully and uniformly enriched both with ^{15}N and ^{13}C could be sufficient to assign all the NMR active half-spin nuclei involved. Because the triple-resonance experiments were not available in the initial stage of this study, we needed to use all three samples.

To discriminate prochiral methyl groups in Val and Leu residues, a sample labeled with ^{13}C by the correlation labeling (Senn et al., 1989) was prepared. Cultivation in the M9 medium containing 30% fully ^{13}C-enriched glucose and 70% nonenriched glucose produced the labeled sample due to asymmetry of biosynthesis. Here, as a natural result, at both the $\gamma 1$ and $\gamma 2$ positions of the Val residues, about 30% were labeled with ^{13}C. For the residue whose $\gamma 1$ position was labeled,

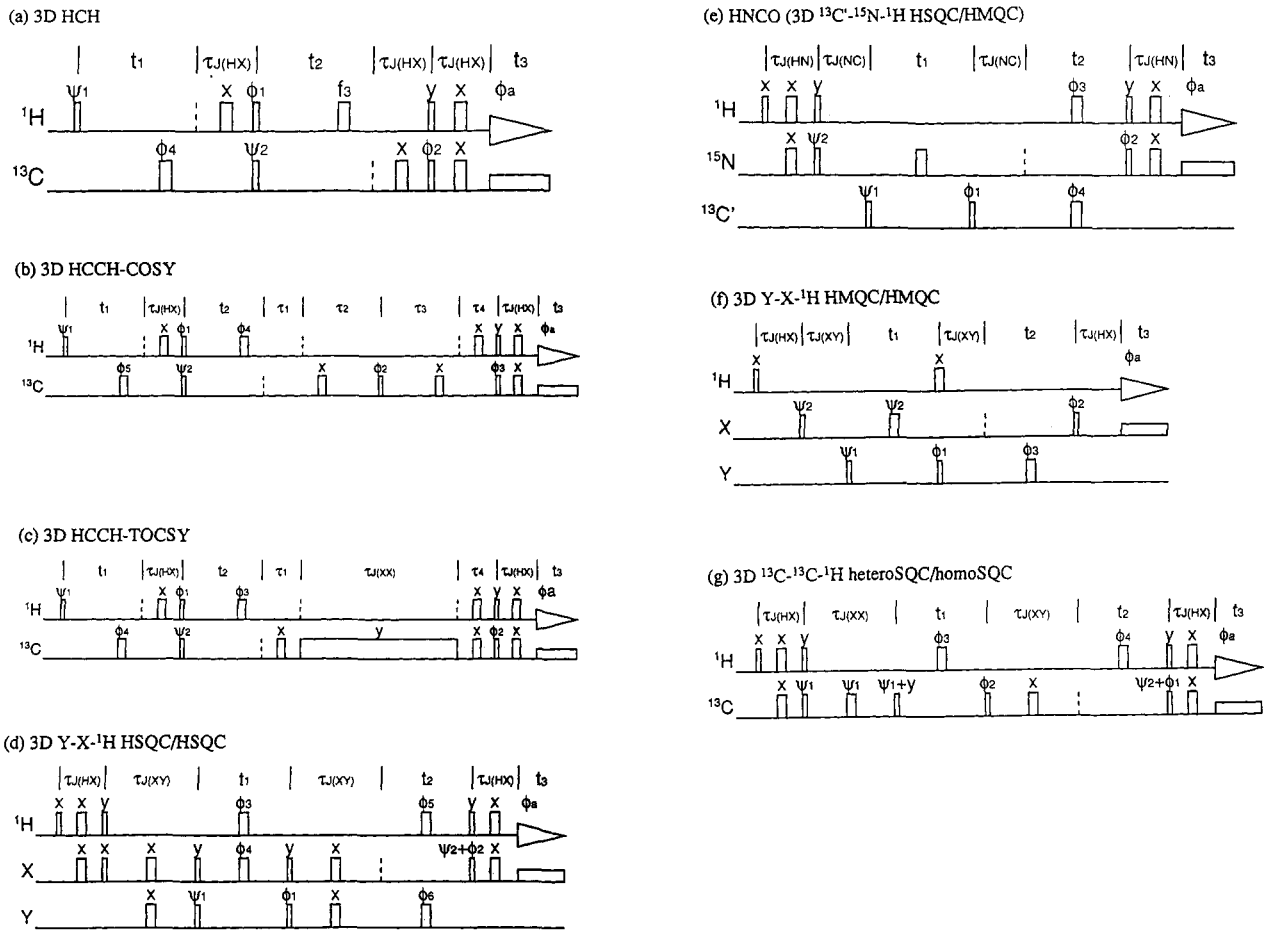

FIGURE 1: Pulse sequences of 3D NMR experiments utilized in this study. The thick bars, thin bars, and broken lines show 180° pulses, 90° pulses, 0° pulses (no pulse), respectively. Triangles indicate data acquisition. Long rectangles represent spin locking or a composite pulse specialized for each purpose. For heteronuclear decoupling, WALTZ-16 is used. Times t_1, t_2, and t_3 vary, while times indicated by τ are fixed. (a) 3D HCH pulse sequence where $\tau_{J(HX)} = \pi/J(HX)$. The inversion pulses for decoupling are located at the centers of $t_1 + \tau_{J(HX)}$ and $t_2 + \tau_{J(HX)}$. Phase cycling is $\phi_1 = (x, -x)$, $\phi_2 = [2x, 2(-x)]$, $\phi_3 = [4x, 4(-x)]$. $\phi_a = (+, -, -, +)$. For complex sets of the first and second dimensions, $\psi_1 = (x, y)$ and $\psi_2 = (x, y)$ are used, respectively. (b) HCCH-COSY pulse sequence where $X = {}^{13}C$, $\tau_{J(HX)} = \pi/J(HX)$, $\tau_1 = \pi/J(HX)/n$ for CH_n, $\tau_4 = \pi/J(HX)/n$ for CH_n, $\tau_2 = \pi/J(XX)/n - \tau_1$ for $C(-C)_n$, and $\tau_3 = \pi/J(XX)/n - \tau_2$ for $C(-C)_n$. The inversion pulses for decoupling are located at the centers of $t_1 + \tau_{J(HX)}$ and $t_2 + \tau_1$. The refocusing pulses are located at the centers of $\tau_1 + \tau_2$ and $\tau_3 + \tau_4$. Phase cycling is $\phi_1 = (x, -x)$, $\phi_3 = [2x, 2(-x)]$, $\phi_2 = [4x, 4(-x)]$, $\phi_4 = [8x, 8(-x)]$, $\phi_5 = [16x, 16(-x)]$, $\phi_a = (+, -, -, +)$. For complex sets of the first and second dimensions, $\psi_1 = (x, y)$ and $\psi_2 = (x, y)$ are used, respectively. (c) HCCH-TOCSY pulse sequence where $X = {}^{13}C$, $\tau_{J(HX)} = \pi/J(HX)$, $\tau_1 = \pi/J(HX)/n$ for CH_n, and $\tau_4 = \pi/J(HX)/n$ for CH_n. The inversion pulses for decoupling are located at the centers of $t_1 = \tau_{J(HX)}$ and $t_2 + \tau_1$. Phase cycling is $\phi_1 = (x, -x)$, $\phi_2 = [2x, 2(-x)]$, $\phi_3 = [4x, 4(-x)]$, $\phi_4 = [8x, 8(-x)]$, $\phi_a = (+, -, -, +)$. For the complex set of the first and second dimensions, $\psi_1 = (x, y)$ and $\psi_2 = (x, y)$ are used, respectively. (d) Y–X–1H HSQC/HSQC pulse sequence where $\tau_{J(HX)} = \pi/J(HX)$ and $\tau_{J(XY)} = \pi/J(XY)$. Phase cycling is $\phi_1 = (x, -x)$, $\phi_2 = [2x, 2(-x)]$, $\phi_3 = \phi_4 = [4x, 4(-x)]$, $\phi_5 = \phi_6 = [8x, 8(-x)]$, $\phi_a = (+, -, -, +)$. For complex sets of the first and second dimensions, $\psi_1 = (x, y)$ and $\psi_2 = (x, -y)$ are used, respectively. (e) HNCO ($^{13}C'$–^{15}N–^1H HSQC/HMQC) pulse sequence where $\tau_{J(HN)} = \pi/J(HN)$ and $\tau_{J(NC)} = \pi/J(NC)$. Phase cycling is $\phi_1 = (x, -x)$, $\phi_2 = [2x, 2(-x)]$, $\phi_3 = [4x, 4(-x)]$, $\phi_4 = [8x, 8(-x)]$, $\phi_a = (+, -, -, +)$. For complex sets of the first and second dimensions, $\psi_1 = (x, y)$ and $\psi_2 = (x, y)$ are used, respectively. (f) Y–X–1H HMQC/HMQC pulse sequence where $\tau_{J(HX)} = \pi/J(HX)$ and $\tau_{J(XY)} = \pi/J(XY)$. 1–1 echo solvent suppression is applied by replacing the first 90° and 180° of the 1H channel by 90°–δ–(–90°) and 90°–2δ–(–90°), where $(\omega_{obs} - \omega_{solv})\ \delta = \pi/2$. Phase cycling is $\phi_1 = (x, -x)$, $\phi_2 = [2x, 2(-x)]$, $\phi_3 = [4x, 4(-x)]$, $\phi_a = (+, -, -, +)$. For complex sets of the first and second dimensions, $\psi_1 = (x, y)$ and $\psi_2 = (x, y)$ are used, respectively. (g) ^{13}C–^{13}C–^1H heteroSQC/homoSQC pulse sequence where $X = {}^{13}C$, $\tau_{J(HX)} = \pi/J(HX)$, and $\tau_{J(XX)} = \pi/J(XX)/n$ for $C(-C)_n$. Phase cycling is $\phi_1 = (x, -x)$, $\phi_2 = [2y, 2(-y)]$, $\phi_3 = [4x, 4(-x)]$, $\phi_4 = [8x, 8(-x)]$, $\phi_a = (+, -)$. For complex sets of the first and second dimensions, $\psi_1 = (x, y)$ and $\psi_2 = (x, -y)$ are used, respectively.

the β position was always labeled. On the other hand, for the residue whose $\gamma 2$ position was labeled, only 30% was labeled at the β position. Carbons of γ, $\delta 1$, and $\delta 2$ positions of the Leu residues were also labeled in the same way.

The enriched proteins were dissolved in H_2O or D_2O buffer adjusted to pH 5.5 with 0.1 M deuteriated acetate. The temperature or the samples during the NMR measurements was at 27 °C. The NMR experiments were done using a GSX-400 spectrometer (JEOL), on which the frequencies were 400 MHz for ^1H, 100.5 MHz for ^{13}C, and 40.5 MHz for ^{15}N nuclei. As described in the previous paper (Yamazaki et al., 1991), a 3D signal is recorded as a series of 2D signal and processed by a home-made software. The spectrometer was modified so that it had a third frequency channel. An external RF power amplifier was required for high-power excitation of the carbon nuclei during a long period of the isotropic mixing in HCCH-TOCSY.

The chemical shifts of ^1H nuclei were measured relative to internal TSP. The chemical shifts of ^{13}C nuclei were measured relative to external TMS in an inner spherical tube. The chemical shifts of ^{15}N nuclei were measured relative to external liquid NH_3 in an inner spherical tube.

A new NMR experiment, 3D HCH, was developed to identify methylene groups in the 3D spectral space. The pulse sequence shown is in Figure 1a, where the magnetization of one of hydrogen nuclei in a methylene group was transferred by one-bond HC spin–spin coupling through the carbon nucleus to the other hydrogen nucleus and then detected. This signal

was modulated by the three chemical shifts of the two hydrogen and one carbon nuclei.

The 3D HCH, HCCH-COSY (Figure 1b), and HCCH-TOCSY (Figure 1c) experiments were done with the sample uniformly enriched with ^{13}C. A typical set of parameters used for 3D HCH was as follows: the observation center was set at 4.78 ppm for ^1H and 50 ppm for ^{13}C; the spectral width was 4.5 ppm (1800 Hz) for f_1 (^1H), 50 ppm (5000 Hz) for f_2 (^{13}C), and 15 ppm (6000 Hz) for f_3 (^1H); the number of 3D complex data points was 64, 32, and 256 for t_1, t_2, and t_3, respectively. Signals were accumulated for 40 h with a repetition rate of 1.1 s. With one zero-filling in each dimension, the final resolution was 14, 78, and 12 Hz for f_1, f_2, and f_3, respectively. The 3D HCCH-COSY experiments with three different sets of mixing times were chosen to optimize parameters for different chemical structures as follows. There were six mixing periods in this pulse sequence, $\tau_{J(HX)}$ ($I^{\pm}_{H1} \rightarrow I^{\pm}_{H1} I^{Z}_{C1}$), τ_1 ($I^{Z}_{H1} I^{\pm}_{C1} \rightarrow I^{\pm}_{C1}$), τ_2 ($I^{\pm}_{C1} \rightarrow I^{\pm}_{C1} I^{Z}_{C2}$), τ_3 ($I^{Z}_{C1} I^{\pm}_{C2} \rightarrow I^{\pm}_{C2}$), τ_4 ($I^{\pm}_{C2} \rightarrow I^{\pm}_{C2} I^{Z}_{H2}$), and $\tau_{J(HX)}$ ($I^{Z}_{C2} I^{\pm}_{H2} \rightarrow I^{\pm}_{H2}$). One set of parameters was for the chemical structure C–CH_2–CH_2–C. The periods τ_1 and τ_4 were set to 1.5 ms and the periods τ_2 and τ_3 to 7 ms. The second one was for the structure $C^{\alpha}H$–$C^{\beta}H_2$–C. The period τ_1 was set to 1.5 ms, the period τ_2 to 7 ms, the period τ_3 to 14 ms, and the period τ_4 to 3 ms. In this experiment, the power of ^{13}C channel was set as the 180° pulses did not excite the carbonyl carbon nuclei, in order to suppress the undesired transfer of the magnetizations of the C^{α} to the C′ nuclei. The last one was for the structure C–CH–CH–C in aromatic groups. The periods τ_1 and τ_4 were set to 3 ms and τ_2 and τ_3 to 4.5 ms. The decoupling channel for carbonyl carbon nuclei was not used. For the isotropic mixing in HCCH-TOCSY, MLEV17 was used. The mixing time was 20 ms for the ^{13}C–^{13}C coherence transfer of the aliphatic side chain nuclei and 10 ms for that of the aromatic nuclei. The power of isotropic mixing was set so that the width of the 90° pulse became 30 μs. A typical set of parameters for 3D HCCH-COSY and 3D HCCH-TOCSY was as follows: the observation center was set at 4.78 ppm for ^1H and 35 ppm for ^{13}C; the spectral width was 7 ppm (2800 Hz) for f_1, 50 ppm (5000 Hz) for f_2, and 15 ppm (6000 Hz) for f_3; the number of 3D complex data points was 64, 32, and 256 in t_1, t_2, and t_3, respectively. Signals were accumulated for 40 h with a repetition rate of 1.1 s. With one zero-filling in each dimension, the final resolution became 22 Hz, 78 Hz, and 12 Hz for f_1, f_2, and f_3, respectively.

For the assignment of the nuclei of the other groups (i.e., some side chain end groups and carbonyl carbons), the approach originally introduced for methods for backbone assignment, HNCA, HNCO, HCACO (Ikura et al., 1990; Kay et al., 1990a), and CT-HCACO (Powers et al., 1991a), was used. In this paper these kinds of pulse sequences are denoted as Y–X–^1H HSQC/HSQC (Figure 1d). HSQC/HMQC (Figure 1e), and HMQC/HMQC (figure 1f). These pulse sequences were compound pulse sequences of two HSQC or HMQC. For example, Y–X HMQC inserted in the t_1 period of X–^1H HSQC makes Y–X–^1H HSQC/HMQC. Here, X and Y represent ^{15}N, aliphatic ^{13}C, or sp^2 ^{13}C (denoted as $^{13}C'$). HNCO and HCACO for the detection of backbone nuclei connectivities were optimized pulse sequences of ^{13}C–^{15}N–^1H HSQC/HMQC and $^{13}C'$–^{13}C–^1H HSQC/HSQC, respectively. In this study, two independent carbon channels for ^{13}C and $^{13}C'$ were not used for the $^{13}C'$–^{13}C–^1H HSQC/HSQC pulse sequence or other pulse sequences with decoupling of the passive coupling. The two kinds of carbon nuclei were managed by a single carbon channel. In the original HCACO pulse sequence (Kay et al., 1990a), the two carbon groups were selectively excited by the "off-resonance DANTE" pulses. But we employed a simpler method, the "1–1" or "1–2–1" pulses. Selective excitation of 90° was realized by 45°–τ–±45°, selective excitation of 180° by 45°–τ–±90°–τ–45°, and excitation for both species by 90°–2τ–90°, where $\tau = \pi/\delta\omega$. Two points should be noted about this treatment. First, the selectivity was not ideal. Aliphatic nuclei that had a nonnegligible offset were also excited to some extent, causing artifacts in the spectrum. They were discriminated by additional phase cycling to the original sequence and setting spectral widths carefully to removed the artifacts around the desired signals. The second point was that a higher power was required for the 1–1 and 1–2–1 pulses than for the off-resonance DANTE. With our spectrometer, the full power of the ^{13}C channel was such that the pulse width of 90° pulses was 17 μs. This was not strong enough to ignore the off-resonance effect. The pulse intervals in the 1–1 and 1–2–1 pulses were set shorter to compensate for this effect.

For the assignment of backbone carbonyl carbon nuclei, HNCO and HCACO experiments (Kay et al., 1990a) were done with the sample doubly enriched with ^{13}C and ^{15}N dissolved in a H_2O buffer and the ^{13}C enriched sample in the D_2O buffer, respectively. The 2D version of HCACO, referred to as $^{13}C'$–(^{13}C)–^1H HSQC/HSQC, was also used to obtain spectra with improved resolution in the carbonyl direction. The parameters for the HNCO experiments were as follows: the observation center was 4.78 ppm for ^1H, 174 ppm for ^{13}C, and 116 ppm for ^{15}N; the spectral width was 15 ppm (6000 Hz) in ^1H, 12 ppm (1200 Hz) in ^{13}C, and 50 ppm (2000 Hz) in ^{15}N; the number of 3D complex data points was 512 in ^1H, 32 in ^{13}C, and 32 in ^{15}N. The mixing time for the ^{13}C–^{15}N coherence transfer was 20 ms. Signals were accumulated 20 h with a repetition rate of 1.1 s. The parameters for HCACO experiments were as follows: the observation center was 4.78 ppm for ^1H and 54 ppm for ^{13}C; the spectral width was 15 ppm (6000 Hz) in ^1H, 50 ppm (5000 Hz) in C^{α}, and 40 ppm (4000 Hz) in C′; the number of 3D complex data points was 256 in ^1H, 32 in C^{α}, 64 in C′. The mixing time for the C^{α}–C′ coherence transfer was 5 ms. Signals were accumulated for 20 h with a repetition rate of 1.1 s. The parameters for the 2D $^{13}C'$–(^{13}C)–^1H HSQC/HSQC experiment were as follows: the spectral width was 90 ppm (9000 Hz) in the C′ direction; the number of data points was 1024; and the resolution after zero-filling was 4.5 Hz. Signals were accumulated for 10 h.

The 2D $^{13}C'$–(^{13}C)–^1H HSQC/HSQC experiments were also used for nonprotonated ^{13}C nuclei in the side chains. For the C^{γ}–C^{β}–H^{β} structure of Asp and Asn residues and the C^{δ}–C^{γ}–H^{γ} structure of Glu and Gln residues, spectra were taken by setting the center of ^{13}C at 37 ppm. For the C^{γ}–C^{β}–H^{β} structure of aromatic residues, the center was set at 33 ppm for $^{13}C^{\beta}$ and 120 ppm for $^{13}C^{\gamma}$. The mixing efficiency from C^{β} to C^{γ} was reduced by the C^{α}–C^{β} coupling. To improve the sensitivity, C^{α} nuclei were decoupled by inserting a 1–1 pulse in the center of the mixing time, adjusting the excitation profile of the 1–1 pulses as a 180° pulse for C^{β} and C^{γ} and a 0° pulse for C^{α}. Since chemical shifts of C^{β} and C^{γ} were different among the Phe, Tyr, Trp, and His residues, different ^{13}C canter frequencies and different intervals of two 90° pulses of 1–1 pulses were used for each of these amino acids.

For the assignment of the N′ nuclei of Pro residues, the N-terminus, and the C63 residue, ^{15}N–^{13}C–^1H HSQC/HSQC experiments (Figure 1d) were used for the sample doubly enriched with ^{13}C and ^{15}N in the D_2O buffer. Since the

homonuclear couplings, C^{α}–C' and C^{α}–C^{β}, which were larger than those of C^{α}–N', impaired the desired coherence transfer, both homonuclear couplings were decoupled by 1–1 pulses inserted in the centers of the C^{α} evolution and the mixing periods. The intervals of 90° pulses in the 1–1 pulses were set as the C^{β} and C' nuclei in the Pro residues were inverted but not C^{α} nuclei. The parameters were as follows: the observation center was at 4.78 ppm for ^1H, 64 ppm for ^{13}C, and 116 ppm for ^{15}N; the spectral width was 15 ppm (6000 Hz) in ^1H, 20 ppm (2000 Hz) in ^{13}C, and 50 ppm (2000 Hz) in ^{15}N; the number of 3D complex data points were 256 in ^1H, 16 in ^{13}C, ar 1 64 in ^{15}N. The mixing time for ^{13}C–^{15}N was 6 ms, which included the ^{13}C evolution time in the constant time mode. Signals were accumulated for 40 h.

A 2D ^{15}N–(^{13}C)–^1H HSQC/HSQC experiment (Figure 1d) for Lys N^{ζ} was done with the following parameters: the observation center was 4.78 ppm for ^1H, 41 ppm for ^{13}C, and 67 ppm for ^{15}N; the spectral width was 74 ppm (3000 Hz) in ^{15}N direction; the number of 2D complex data points was 256 in the ^{15}N direction and 512 in the ^1H direction. The mixing time for the ^{13}C–^{15}N coherence transfer was 28 ms, in which magnetizations would be fanned out and refocused into in-phase coherences by the scalar coupling between C^{γ} and C^{ϵ}.

The C^{ζ} nuclei of Arg residues were detected in the HNCO (^{13}C–^{15}N–^1H HSQC/HMQC) spectra explained above. Some H^{ϵ} nuclei were exchanging with solvent protons at high rates, and then the corresponding peaks were observed to vanish. To detect these with sufficient sensitivity, 2D ^{13}C–(^{15}N)–^1H HMQC/HMQC (figure 1f) with a 1–1 echo solvent suppression was used. The C^{γ} nuclei was decoupled during the ^{15}N–^{13}C mixing period. The parameters were as follows: the observation center was at 4.78 ppm for ^1H, 159.4 ppm for ^{13}C, and 88.8 ppm for ^{15}N; the spectral width was 27.4 ppm (2750 Hz) in f_1 (^{13}C) and 15 ppm (6000 Hz) in f_2; the number of 2D complex data points was 128 in t_1 and 512 in t_2. The observation center of the 1–1 echo filter was set at 7.8 ppm. The mixing time for the ^{13}C–^{15}N coherence transfer was 20 ms.

The heteroSQC/homoSQC, a homonuclear version of HSQC/HSQC experiment, was newly developed as shown in Figure 1g. This was applied to detect ^1H–^{13}C–^{13}C substructures in aromatic rings, in which structure no protons are attached to the latter carbon. In the spectra of this 3D NMR, positive cross peaks $X(^{13}C)$–$Y(^{13}C)$–$Z(^1H)$ and negative diagonal peaks $Y(^{13}C)$–$Y(^{13}C)$–$Z(^1H)$ were observed. The experiment was applied to the sample uniformly enriched with ^{13}C in the D_2O buffer. The parameters were as follows: the observation center was at 132.5 ppm for ^{13}C and 4.78 ppm for ^1H; the spectral width was 60 ppm (6000 Hz) in f_1, 30 ppm (3000 Hz) in f_2, and 15 ppm (6000 Hz) in f_3; the number of 3D complex data points was 64 in t_1, 32 in t_2, and 256 in t_3. The mixing times for the ^{13}C–^{13}C coherence transfer were 2.4 ms. Signals were accumulated for 40 h with a repetition rate of 1.1 s.

A 2D ^{15}N–^1H HMQC experiment was applied to the sample uniformly enriched with ^{15}N in the D_2O buffer to detect the $N^{\delta 1}$ and $N^{\epsilon 2}$ nuclei of His residues. Correlation peaks between the two nitrogen nuclei and the two proton nuclei, $H^{\epsilon 1}$ and $H^{\delta 2}$, through $^2J_{NH}$ and $^3J_{NH}$ were observed in this spectrum. The decoupling of ^{15}N nuclei during the acquisition period was not employed. The mixing times for the ^1H–^{15}N coherence transfer was 15 ms, which was three times longer than that for direct ^1H–^{15}N coupling, because $^2J_{NH}$ and $^3J_{NH}$ were much smaller than $^1J_{NH}$. The observation center was at 4.78 ppm for ^1H and 165.4 ppm for ^{15}N. The spectral width was 200 ppm (8000 Hz) in f_1 and 15 ppm (6000 Hz) in f_2. Data of 512 complex points by 512 complex points was acquired. After one zero-filling in each of the dimensions, the final resolution was 7.8 and 5.9 Hz for f_1 and f_2, respectively.

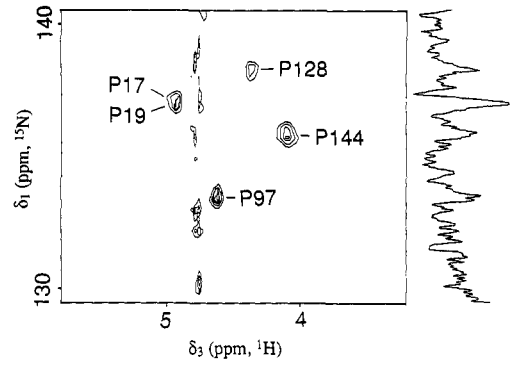

FIGURE 2: Superimposed slices for the N'–H^{α} of Pro residues taken from a 3D ^{15}N–^{13}C–^1H HSQC/HSQC spectrum. Planes of ^{13}C chemical shifts of 64.5 ~ 67.0 ppm are selected. The 1D spectrum on the right side is from the direct observation of ^{15}N.

RESULTS

Backbone Carbonyl Carbon Nuclei Assignments. Based on the knowledge of the chemical shifts of H^{α} and C^{α} (Yamazaki et al., 1991), chemical shifts of carbonyl carbon nuclei were determined through *J* connectivities between C^{α} and C' nuclei. Connectivities of H^{α}–C^{α}–C' in the same residues were obtained from the 2D $^{13}C'$–(^{13}C)–^1H HSQC/HSQC and 3D HCACO spectra. Owing to the very sharp resonance of C', the 2D peaks were resolved well on the $^{13}C'$–(^{13}C)–^1H spectrum. All of the resonances except for about 10 overlapping peaks were assigned. The overlapping peaks were also distinguished by their connectivities to N' of the residues next to the C' nuclei that were revealed in the 3D HNCO spectrum. In our previous experiments, sequential connectivities between residues had been determined through NOE connectivities between the H^{α} and H^N nuclei of sequential residues. These were all confirmed by the assignment techniques shown here. The chemical shifts of the C^{α} of the Ile, His, Leu, and Val residues, which had not been determined in the previous study because of labeling defects, were also determined in this study.

Backbone Nitrogen Nuclei Assignments. All but seven backbone nitrogens had already been assigned in the previous work. The unassigned ones were those of Pro residues, the N-terminus, and residue C63, because the amide protons of these residues were not observed or because they did not exist. The assignments were obtained by *J* connectivities were N' and C^{α} nuclei that were revealed in the 3D ^{15}N–^{13}C–^1H HSQC/HSQC spectrum. The N-terminus and C63 amide nitrogens were thus assigned. In the 3D spectrum, only four Pro nitrogen peaks out of five appeared with distinct chemical shifts from other amide nitrogens as shown in Figure 2. The chemical shifts of N', C^{α}, and H^{α} of P17 and P19 were found to have degeneracy. This degeneracy was confirmed with 1D ^{15}N experiments, where the degenerate peak appeared with an intensity twice as high as that of other peaks of single nitrogens.

Aliphatic Side Chain Nuclei Assignments. The hydrogen and carbon nuclei in the aliphatic parts of the side chains were assigned from the previously assigned C^{α} through *J* connectivities between carbons covalently bonded in the side chains. The single *J* connectivities of two adjacent carbons were revealed in the 3D HCCH-COSY spectrum. Severe over-

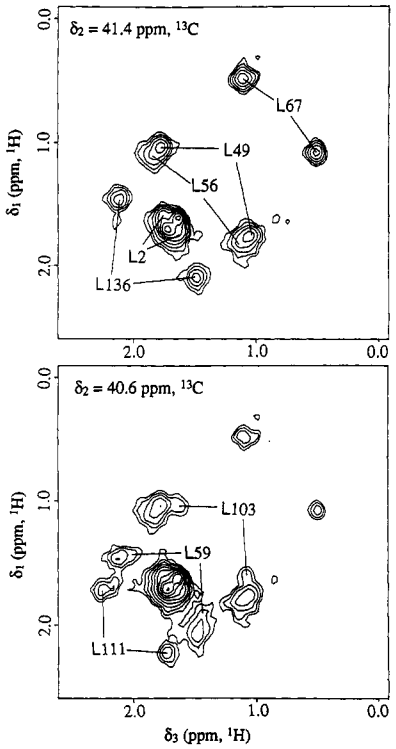

FIGURE 3: Slices taken from a 3D HCH spectrum. A region for the $C^{\beta}H_2$ of Leu residues is selected. The two slices are neighboring ones.

lapping of the aliphatic carbon and hydrogen chemical shifts, however, prohibited us for connecting them to the ends of carbon chains in the side chains. The 3D HCCH-TOCSY method solved this problem. In this spectrum, through multiple ^{13}C–^{13}C J connectivities, carbon and hydrogen nuclei at γ, δ, and ϵ positions were directly connected to C^{α} nuclei whose chemical shifts were less overlapped. Another difficulty in the assignments of aliphatic chains came from methylene groups. One of the two hydrogen resonances was easily lost when the chemical shifts of the two protons were largely separated or when one of them was overlapped by other peaks. The 3D HCH experiment solved this problem, where peaks of methylene groups representing hydrogen pairs appeared with high sensitivity. This spectrum was helpful in assignment of the $C^{\gamma}{}^{1}H_2$ groups of Ile residues, $C^{\beta}H_2$ of Leu residues as shown in Figure 3, and methylene hydrogens that had unusual chemical shifts as described in the following paragraphs.

Side chain carbon and hydrogen ncclei of residues with short side chains and methyl groups (Ala and Thr) were able to be assigned only by their ^{1}H–^{1}H J connectivities in the 3D ^{13}C–^{1}H–^{1}H HMQC-TOCSY spectra, by which the backbone assignment had also been done. In all cases, however, 3D HCCH-COSY and 3D HCCH-TOCSY were much more sensitive. Here, assignments of side chain nuclei by using 3D HMQC-TOCSY are not used. The $C^{\beta}H_3$ groups of Ala residues were assigned only with 3D HCCH-COSY. The $C^{\beta}H$ and $C^{\gamma}H_3$ nuclei in Thr residues were assigned with 3D HCCH-COSY. The chemical shifts of H^{α} and H^{β} of T42 and T79 were eventually very close, but their assignments were completed with the aid of 3D HCCH-TOCSY.

The $C^{\beta}H$ and $(C^{\gamma}H_3)_2$ groups in Val residues were assigned with 3D HCCH-TOCSY. The single J connectivities of $C^{\alpha}H$–$C^{\beta}H$ in Val residues were weak in 3D HCCH-COSY due to 2-fold passive couplings to the two C^{γ} nuclei. The connectivities were observed with better sensitivity in 3D HCCH-TOCSY. The $C^{\beta}H$, $C^{\gamma 2}H_3$, and $C^{\delta 1}H_3$ of Ile residues were assigned with 3D HCCH-TOCSY. The single J connectivities of $C^{\alpha}H$–$C^{\beta}H$ in 3D HCCH-COSY were also weak for the same reason mentioned above. The $C^{\gamma}{}^{1}H_2$ methylene groups were assigned with 3D HCCH-COSY and 3D HCH spectra. The $C^{\gamma}H$, $C^{\beta}H_2$, and $(C^{\delta}H_3)_2$ nuclei of Leu residues were assigned with 3D HCCH-TOCSY. Cross peaks arising from $C^{\beta}H_2$ were very weak, but their assignments were confirmed with 3D HCH.

Table I: Chemical Shifts of Ring ^{13}C and ^{15}N Nuclei of His Residues in RNase H Compared with Histidine Limiting Shifts

	C^{γ}	$C^{\delta 2}$	$C^{\epsilon 1}$	$N^{\delta 1}$	$N^{\epsilon 2}$
His[a]	133.7	119.6	137.8	223.3	179.2
H114	134.7	116.5	138.7	247.7	163.1
H83	130.0	117.8	135.4	198.1	175.3
H124	129.9	117.3	134.8	182.3	174.3
H62	129.0	118.5	134.4	177.5	174.3
H127	129.2	119.5	134.4	177.3	175.8
His^{+} [b]	129.5	119.0	135.2	181.5	183.2

[a] Chemical shifts of histidine in the basic state (the $N^{\epsilon 2}H$ form). [b] Chemical shifts of histidine in the acidic state (the $N^{\delta 1}H$–$N^{\epsilon 2}H$ form) (Martin et al., 1981).

The $C^{\beta}H_2$ groups in the Cys, Asp, Asn, and Ser residues were assigned with 3D HCCH-COSY, where the connectivities appeared with high sensitivity. The $C^{\beta}H_2$ groups in the aromatic residues Phe, His, Tyr, and Trp were assigned with 3D HCCH-COSY and 3D HCH. The $C^{\alpha}H$–$C^{\beta}H_2$ connectivities were very weak due to J couplings between C^{β} and C^{γ} nuclei. The missing connectivities were recovered by replacing at 180° pulse by a semiselective pulse (two 90° pulses with an appropriate interval) which flipped C^{β} nuclei at 180° and C^{γ} nuclei at 0°. In spite of the improvement, peaks from one of two protons of W81 (1.74/0.67 ppm) and from one of two protons of W118 (2.30/1.38 ppm) escaped my notice at first, because of their unusual upfield shifts. They were found in 3D HCH spectrum and assigned. On the other hand, chemical shifts of $H^{\beta}{}_2$ of W90 showed unusual downfield shifts (3.26/3.46 ppm).

The $C^{\beta}H_2$ and $C^{\gamma}H_2$ groups in the Glu, Gln, and Met residues were assigned with 3D HCCH-TOCSY. The C^{β}, H^{β}, C^{γ} of E131 and E135 were overlapped in addition to the overlappings of their C^{α}, H^{α}, and N^{N}. The $C^{\epsilon}H_3$ nuclei of Met residues were assigned with NOE connectivities of $H^{\epsilon}{}_3$–H^{N} and/or $H^{\epsilon}{}_3$–H^{α} found in the 3D ^{13}C–^{1}H–^{1}H HMQC-NOESY spectra.

All the hydrogen and carbon nuclei of the methylene groups of the Lys residues were assigned with 3D HCCH-TOCSY. The $C^{\epsilon}H_2$ of all but K3 had very similar chemical shifts to each other. All the hydrogen and carbon nuclei of the methylene groups of the Arg residues except R46 were assigned with 3D HCCH-TOCSY. One of two H^{γ} protons of R75 (0.40/–0.70 ppm) were found to be shifted strongly upfield. Though it gave a very weak peak in the 3D HCCH-TOCSY spectrum, it was confirmed with 3D HCH. The $C^{\beta}H_2$ and $C^{\gamma}H_2$ of R46 were not assigned because their peaks were not identified.

The methylene hydrogen and carbon nuclei of Pro residues were assigned with 3D HCCH-TOCSY. The assignments of $H^{\delta}{}_2$ were also confirmed with NOE connectivities. For all but P17, NOE connectivities between the $H^{\delta}{}_2$ nuclei of the Pro residues and the H^{α} nuclei of the preceding residues were observed. The P17 residue was found to take a *cis*-Pro form form because of a strong NOE connectivity observed between the H^{α} of N16 and the H^{α} of P17. The other Pro residues take the usual *trans* conformation.

Table II: Averages and rmsds (in Parentheses) of Secondary Shifts in Secondary Structures of RNase H

structure	no. of residues	C^α	C^β	C'	N'	H^α	H^N
α-helix	51	2.4 (1.2)	−1.3 (1.2)	2.1 (1.4)	−4.5 (3.4)	−0.53 (0.37)	−0.36 (0.63)
β-strand	36	−1.69 (0.8)	1.43 (1.3)	−1.01 (1.3)	1.1 (4.0)	0.58 (0.43)	0.32 (0.61)
all	132[a]	0.29 (2.2)	−0.43 (2.2)	0.49 (1.9)	−2.1 (4.9)	−0.06 (0.61)	−0.11 (0.71)

[a] N-Terminal, Gly, Pro, and Cys residues are excluded.

Table III: Secondary Shifts of Backbone Nuclei of the Residues That Have Positive ϕ Angles in RNase H

residue no.	R29	G89	W90	K95	N100
ϕ	7.39	68.0	59.2	64.6	58.6
ψ	−125.3	35.6	47.0	29.0	31.1
C^α	0.5	0.5	−0.5	1.2	1.6
C^β	−3.4	-[a]	−6.1	−4.9	−2.9
C'	1	0.9	−1.2	−1.4	0.9
N'	0.6	−2	−10.8	−13	−7.4
H^α	−0.6	−0.04	−1.28	−0.69	−0.47
H^N	1.1	−0.61	0.47	−0.35	0.7

[a] No C^β.

Side Chain Carboxyl and Carbonyl Carbon Nuclei Assignments. With the same strategy as that used for the backbone carbonyl carbon assignments, side chain carboxyl carbon nuclei as Asp and Glu and carbonyl carbon nuclei of Asn and Gln residues were assigned from side chain methylene groups through single ^{13}C–$^{13}C'$ J connectivities. The 2D $^{13}C'$–(^{13}C)–^1H HSQC/HSQC spectrum had a resolution good enough to distinguish all of the peaks, as shown in Figure 4. Though the chemical shifts of H^{γ_2} of Q4 and Q113 were very close, they were distinguished by using the chemical shifts in C^γ in the 3D HCACO spectrum, which was taken for the assignments of backbone carbonyl carbons.

Side Chain Amide Nitrogen and Hydrogen Nuclei Assignments. The 3D HNCO spectrum used for the connectivities of backbone nuclei also showed peaks from the side chain amide groups of Asn and Gln residues. They were assigned from side chain carbonyl carbons through J connectivities. The amide hydrogens of Q105 showed unusual shifts (6.54/5.08 ppm), one of which was largely shifted in the upfield direction close to that of the water signal. It was, therefore, assigned with the help of a 3D ^1H–^{15}N–^1H TOCSY-HMQC spectrum. Only one single peak for the N100 side chain amide protons was observed. This was confirmed to be degenerate, because it they became two separated peaks when KCl was added (Oda et al., 1991).

Aromatic Hydrogen, Carbon, and Nitrogen Nuclei Assignments. The C^γ nuclei of aromatic residues His, Tyr, Phe, and Trp were assigned from $C^\beta H_2$ through H^β–(C^β)–C^γ J connectivities revealed with the 2D $^{13}C'$–(^{13}C)–^1H HSQC/HSQC spectra, where the passive couplings with the C^α nuclei were decoupled. Peaks of His residues were split in the direction of the ^{13}C axis by one passive coupling with the $C^{\delta 2}$. Those of the other aromatic residues were much weaker due to the multiple splitting from two passive couplings with the neighboring carbons in the aromatic rings. The chemical shift of C^γ (134.7 ppm) in H114 was unusual, indicating an interesting chemical aspect as discussed later. The peaks from Y28 and Y151 were very close. The $C^\delta H$ of Phe and Tyr, $C^{\delta 1}H$ of Trp, and $C^{\delta 2}H$ of His residues were assigned from the C^γ nuclei through connectivities between C^γ and C^δ obtained by the ^{13}C–^{13}C–^1H heteroSQC/homoSQC method. The resultant assignments coincided with those obtained by NOE connectivities between H^β and H^δ. Other aromatic carbon and hydrogen nuclei were connected with the HCCH-COSY and HCCH-TOCSY spectra. The aromatic nitrogen nuclei of His residues were assigned with ^{15}N–^1H HMQC spectrum. Two nitrogen nuclei, $N^{\epsilon 2}$ and $N^{\delta 1}$, were distinguished by J coupling constants to $H^{\delta 2}$ with the assumption that $^2J(H^{\delta 2},N^{\epsilon 2})$ is larger than $^3J(H^{\delta 2},N^{\delta 1})$ (Oh et al., 1990; Blomberg & Rüterjans, 1983). The chemical shift of $N^{\delta 1}$ of H114 was shifted 60 ppm downfield from the other peaks. That of H114 was unusual in the acidic solution, but rather typical in the neutral state of the His residue. Nonprotonated carbons, C^ζ of Tyr and $C^{\delta 2}$ and $C^{\epsilon 2}$ of Trp, were assigned with the ^{13}C–^{13}C–^1H heteroSQC/homoSQC method. In this spectrum, the C^ζ–C^ϵ–H^ϵ connectivities of the Tyr residues, as shown in Figure 5, and the $C^{\epsilon 2}$–$C^{\zeta 2}$–$H^{\zeta 2}$ and $C^{\delta 2}$–$C^{\epsilon 3}$–$H^{\epsilon 3}$ connectivities of the Trp residues appeared; however, the last connectivities were always weak. This weak intensity was caused by the strong coupling between $C^{\epsilon 3}$ and $C^{\zeta 3}$ and by the passive coupling of $C^{\delta 2}$ to $C^{\epsilon 2}$, C^γ, and $C^{\epsilon 3}$. All of the chemical shifts of $C^\delta H$, $C^\epsilon H$, and $C^\zeta H$ of the two Phe residues were too close to be assigned separately even with the 3D spectra. In the ^{13}C–^1H HMQC spectra of the sample prepared by the correlation labeling, the coupling patterns of the C^δ nuclei of Tyr and Phe residues were simplified to doublets, which were, on the other hand, double-doublets in the fully enriched samples. The $C^\delta H$ nuclei of Phe residues were then identified with the HMQC spectra and were assigned with the help of intraresidue NOE cross peaks.

Guanidino Nuclei of Arg and Amino Nuclei of Lys Assignments. The C^ζ nuclei of Arg residue were assigned with the ^{13}C–^{15}N–^1H HSQC/HSQC method. Since the H^η nuclei of Arg residues were very labile, the $N^\eta H_2$ peaks in ^{15}N–^1H HMQC were observed, but they were very weak. Most of them appeared at 6.6 ~ 6.9 ppm (^1H) and 70 ~ 73 ppm (^{15}N). Hence, they were not discriminated except for two $N^\eta H_2$ groups, one of which was assigned to R46 by the NOE connectivity from R46 H^ϵ. The N^ζ nuclei of Lys residues were observed with the ^{15}N–^{13}C–^1H HSQC/HSQC method. Their chemical shifts were too close (30.8 ~ 31.5 ppm ^{15}N), however, to be distinguished except for K3, K33, and K117 out of the 11 residues.

The number of magnetically distinguishable nuclei in this enzyme amounts of 1962 (227 nitrogens, 762 carbons, and 973 protons). Among them a total of 1858 nuclei (95%) (200 nitrogens, 749 carbons, and 919 protons) were assigned. All of the chemical shifts of these nuclei are listed in Table IV in the Appendix.

DISCUSSION

Almost all of the ^1H, ^{13}C, and ^{15}N nuclei of RNase H from *E. coli* that are detectable by NMR were assigned. In a separate study, a very limited number of methyl protons and aromatic protons had been assigned by the conventional COSY and 3D TOCSY methods. Amino acid selective ^1H labeling of a perdeuterated protein sample also allowed assignments of nuclei in the labeled residues (Oda et al., 1992). The assignment strategy utilized here with the 3D NMR experiments of uniformly enriched samples is overwhelmingly

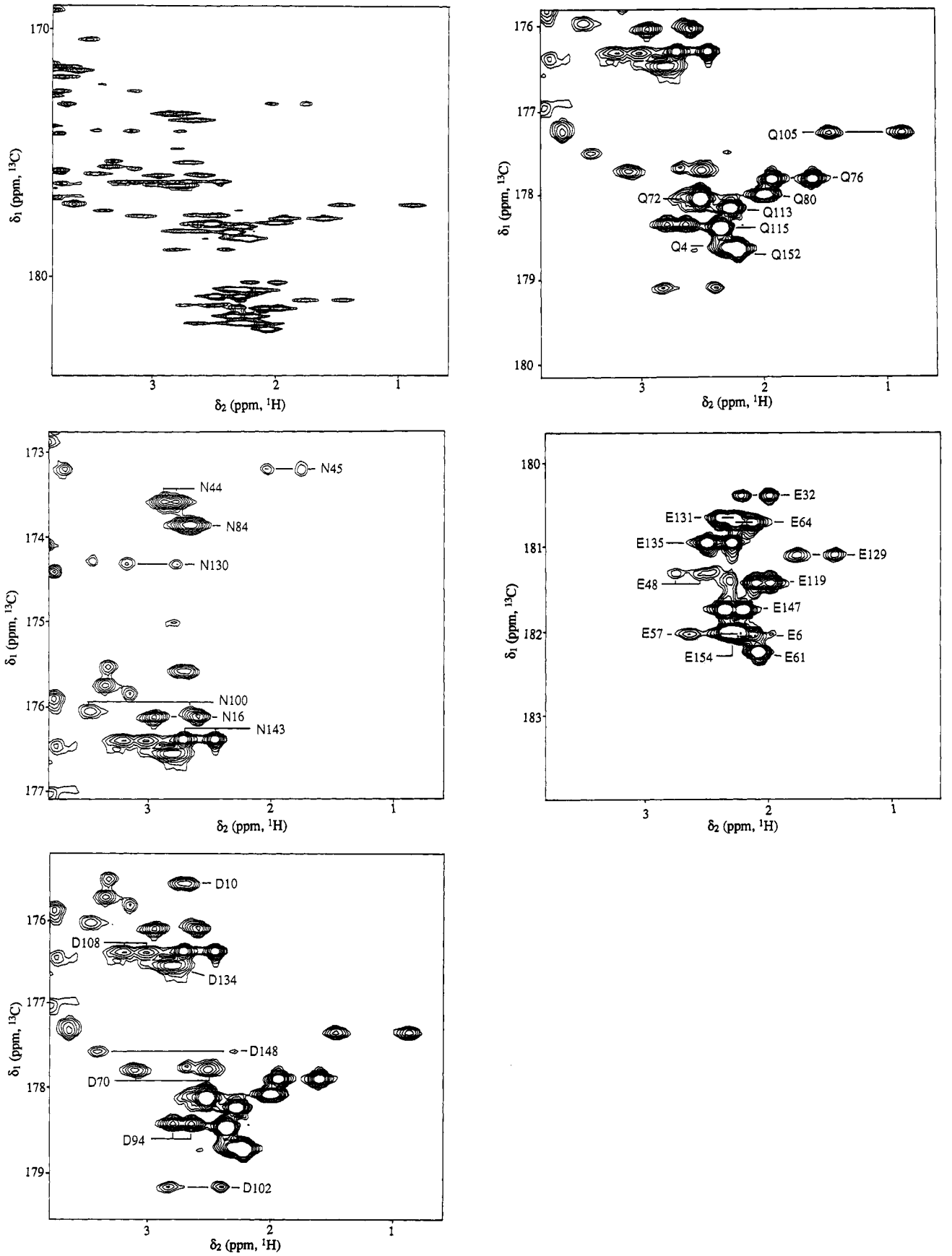

FIGURE 4: Side chain carbonyl and carboxyl carbon peaks in a 2D $^{13}C'$–(^{13}C)–^{1}H HSQC/HSQC spectrum. The entire region for side chain carbons is shown in panel a (top left). Assignments of Asn (b, middle left), Asp (c, bottom left), Gln (d, top right), and Glu (e, bottom right) are shown in the expanded spectra.

powerful. However, there are several defects in the assignment even in this comprehensive study. We shall first summarize the unassigned nuclei and give the reasons.

None of the $(N^{\eta}H_2)_2$ groups of the Arg residues, except for R46, were assigned. Since two nitrogens and four protons in this group are distinguishable, the 10 Arg residues in this

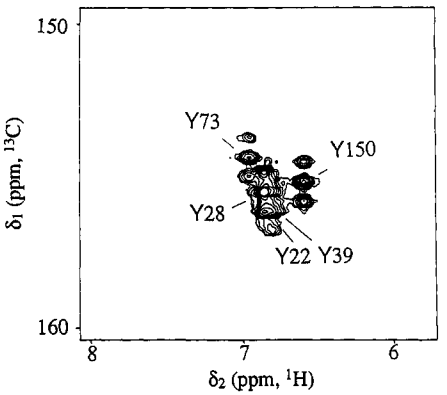

FIGURE 5: Tyr C^{ζ} assignments on a 2D ^{13}C–(^{13}C)–^{1}H heteroSQC/homoSQC spectrum. The correlation peaks C^{ζ}–(C^{ϵ})–H^{ϵ} of Tyr residues are shown.

protein give 40 proton and 20 nitrogen resonances. But, in the solution with a pH of 5.5, the higher exchange rates of the protons make the intensities of NH_2 peaks weaker. Moreover, the two $N^{\eta}H_2$ groups of arginine amino acid are not distinguished (Blomberg & Rüterjans, 1983). It was very difficult to assign all of $(N^{\eta}H_2)_2$ groups in this solution because of the weak intensities and severe overlapping of the peaks. Only two peaks of the $N^{\eta}H_2$ groups were distinct in the ^{15}N–^{1}H HMQC spectra. One of them was assigned to a $N^{\eta}H_2$ group of R46 through its NOE connectivity with $N^{\epsilon}H$. The $N^{\eta}H_2$ group, among the two groups of R46, must be the closer NH_2 group to the H^{ϵ}. The other peak can be assigned to the other $N^{\eta}H_2$ group of R46 with NOE connectivity to the H^{α} of N100, if the protein structure determined by crystallography is assumed. All of the chemical shifts of the $N^{\eta}H_2$ groups of the remaining Arg residues are in the region of 6.6 ~ 6.9 ppm for ^{1}H and 70 ~ 73 ppm for ^{15}N. The next major deficiency was assignment of the Lys N^{ζ} nuclei, which were also severely overlapped except for the three residues K3, K33, and K117. All of the others are in the range 30.8 ~ 31.5 ppm. Peaks from the Trp $C^{\delta 2}$ nuclei, to which no proton attached, were very weak. Those of W81, W104, and W118 were not assigned because the corresponding peaks were not observed. The low sensitivities of these carbons originate from the passive couplings with three connected spins and the ineffective coherence transfer due to the strong coupling compared to the small chemical shift difference between the $C^{\epsilon 3}$ and $C^{\zeta 3}$ nuclei. The $C^{\epsilon 3}H$ of W81, the $C^{\epsilon 3}H$ and $C^{\zeta 3}H$ of W104, and the $C^{\delta}H$, $C^{\epsilon}H$, and $C^{\zeta}H$ of F8 were not assigned due to overlapping. Peaks from the $C^{\beta}H_2$, $C^{\gamma}H_2$ of R46, the $C^{\beta}H_2$, $C^{\gamma}H_2$ of M47, and the $C^{\beta}H_2$ of E48 were not identified in the 3D HCCH-TOCSY spectrum, probably due to faster transverse relaxations. It is interesting to consider that this region, which is a part of the catalytic site, has distinct dynamics that are different from the rest of the molecule.

Next, we shall discuss the overall characteristics of the chemical shifts of carbon and nitrogen nuclei obtained in this study. An average and a dispersion of chemical shifts at each position in each amino acid were calculated. The results are summarized in Figure 6. For the ^{13}C chemical shifts, large dispersions are mainly observed in the backbone nuclei, C^{α},

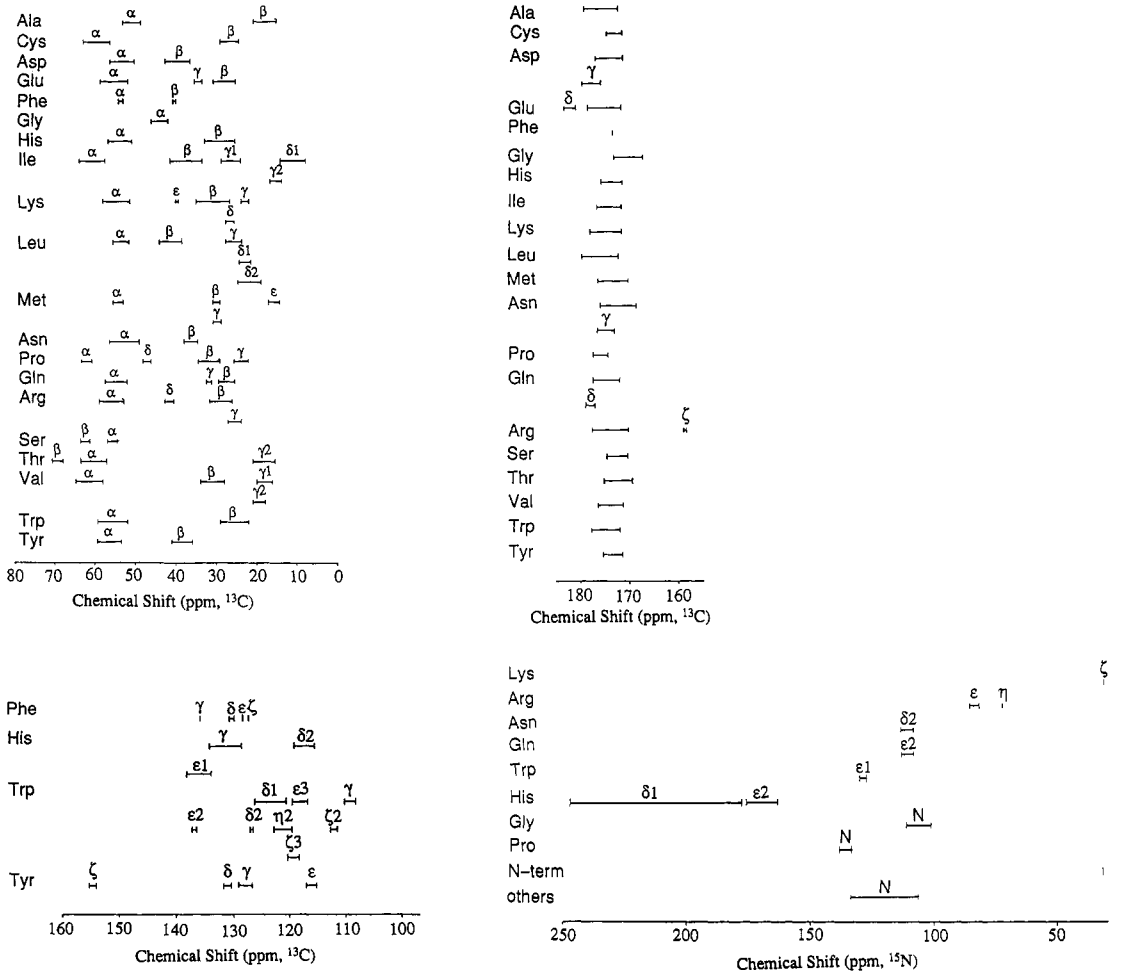

FIGURE 6: (a, top left) Aliphatic ^{13}C, (b, top right) carbonyl ^{13}C, (c, bottom left) aromatic ^{13}C, and (d, bottom right) ^{15}N chemical shift distributions for each nucleus of 20 amino acids.

C^{β}, and C′. This suggests that local backbone structures contribute largely to the secondary shifts. On the contrary, the ^1H chemical shifts both of the side chain nuclei and backbone nuclei have shown large dispersions. For example, one of the two H^{γ} nuclei of R75 had the highest field chemical shift (–0.7 ppm) among all ^1H nuclei, which would be explained by the ring current effect from W120.

The chemical shifts of the His $N^{\delta 1}$ nuclei have an extremely large dispersion of 70.4 ppm. Among them, only H114 has a distinct chemical shift. A His residue can exist in any one of three tautomers: the state protonated both at $N^{\delta 1}$ and $N^{\epsilon 2}$ (positively charged), the $N^{\delta 1}H$ state, or the $N^{\epsilon 2}H$ state. In a solution of pH 5.5, His residues are normally protonated at both positions. For a histidine (amino acid form), the $N^{\epsilon 2}H$ state dominates in basic solutions (Kawano & Kyogoku, 1975). The chemical shifts of the nitrogen and carbon nuclei of the H114 residue are similar to those of histidine in basic solution, and the others are similar to those of histidine in acidic solution as shown in Table I. It is concluded, therefore, that only H114 is in the $N^{\epsilon 2}H$ state and the others are in the positively charged state.

The peptide bond preceding P17 is found to have the *cis* conformation, based on the NOE connectivity between N16 $C^{\alpha}H$ and P17 $C^{\alpha}H$. For the other Pro residues, the NOE connectivities between the $C^{\delta}H_2$ of the Pro residues and $C^{\alpha}H$ of the preceding residues are all consistent with those expected from *trans*-prolines. It is interesting and notable that the chemical shifts of N′, C^{α}, and C^{δ} nuclei of a Pro residue are not affected by the *cis–trans* conformation change of the peptide bond, but those of C^{γ} and C^{β} are affected to some extent even though they are located farther from the peptide bond.

A mechanism of enzymatic catalysis where one of the Glu or Asp residues should is in the protonated state was proposed (Nakamura et al., 1991). The chemical shift of the C^{γ} of Asp residue in the random coil state is 178.5 ppm for the deprotonated (negatively charged) state and 175.0 ppm for the protonated state. The C^{γ} nuclei of D10, D108, and D134 showed chemical shifts close to that of the protonated state. The residue D10, which is a crucial residue for catalysis, is a hopeful candidate for the proton donor. But the difference of the chemical shifts between the protonated and deprotonated states is too small to identify the states without an appropriate experiment using pH titration, which will be reported soon (Oda et al., manuscript submitted).

The secondary shifts, which are the differences from the chemical shifts in the random coil state (Wüthrich, 1986; Richarz & Wüthrich, 1978; Glushka et al., 1989a,b), were calculated to find their correlation to the structure of the protein molecule. All of the random coil shifts, except for the ^{13}C shifts of reduced Cys, ^1H shifts of His in the charged and $N^{\epsilon 2}H$ state, ^1H shifts of *cis*-Pro, and ^{15}N shifts of sidechains, have been obtained from the reports. The residue P17 and H114 are distinguished from other Pro and His residues for the reason that they are in unique states.

A fairly strong correlation between the secondary structures and the secondary shifts of the backbone nuclei N′, H^N, C^{α}, H^{α}, C^{β}, and C′ is observed. The residues are divided according to secondary structures: 53 residues in α-helices, 42 residues in β-strands, and others. Averages and rooted mean square deviations (rmsd) of the secondary shifts of the residues taking the secondary structures are listed in Table II. In particular, the difference of the average chemical shifts of the C^{α} in α-helices and in β-strands is two times as large as the dispersions in each class, indicating that the carbon chemical shifts become a good measure for the secondary structures. There are also clear differences between the two structures in the chemical shifts of C^{β}, C′, and H^{α}. These chemical shifts can be also used for the identification of the secondary structure by combining those of neighboring residues (Wishart et al., 1992). But those of N′ and H^N do not provide a clear measure for the secondary structure identification. In the comprehensive work of chemical shift analyses recently reported (Wishart et al., 1991), the chemical shifts of the N′ and H^N nuclei have been reported to correlate to their hydrogen-bonding energies. It is, however, a difficult work to separate the contribution of hydrogen bonding from that of the secondary structure, since hydrogen-bonding energies for atoms on the surface of the molecule can not easily be evaluated due to the loose hydrogen bonds to water molecules.

The C^{β} of W90 showed the largest secondary shift (6.1 ppm upfield) among the carbon nuclei. This residue is found to be in a left-handed helix structure by the X-ray crystallographic studies. There are six residues whose ϕ angles are positive, R29, G89, W90, K95, N100, and V155. Among them, V155 at the C-terminus and G89 with no C^{β} are not interesting. R29 is involved in type II β-turn, W90, K95, and N100 in left-handed α-helices. The chemical shifts of C^{β} nuclei of the four residues are interestingly all shifted the most in the upfield direction, as listed in Table III. A data base analysis published recently has also shown upfield shift (Spera & Bax, 1991), but it is smaller than those obtained in RNase H. A theoretical calculation of C^{β} chemical shifts dependent on the backbone local conformation (Ando et al., 1984) does not show any difference between right- and left-handed helices. It should be noted that their backbone N′ nuclei were correspondingly shifted largely to the upfield. It is confirmed with strong intraresidue H^N–H^{α} NOE connectivities that these residues exist in left-handed helical structures in a solution state, as well as in the crystal.

The H^{ϵ} of R46 showed the largest secondary shift (2.97 ppm downfield) among the ^1H nuclei. The X-ray structure showed a strong hydrogen-bonding network around R46. The H^{ϵ} and $H^{\eta 2}$ were connected to the two O^{δ} of D148, and the $H^{\eta 1}$ and $H^{\eta 2}$ were connected to the two O^{δ} of D102. R106 also shifted to the downfield (1.37 ppm), and hydrogen bonding of H^{ϵ} and $H^{\eta 2}$ to the two O^{ϵ} of E57 was found. The effects of this hydrogen bonding on chemical shifts of the side chain carboxyl carbons of D102, D148, and E57 were not clear compared with those on the hydrogen chemical shifts.

CONCLUSION

The assignment of the ^1H, ^{13}C, and ^{15}N nuclear magnetic resonances of ribonuclease H from *E. coli* was completed using triple-resonance 3D NMR techniques. The results contain almost all of the half-spin nuclei (95%) that are detectable by NMR. The chemical shifts are found to be a good measure of local structures and charged states by their secondary shifts. This result can be used to elucidate fine changes in the molecular structure in the solution state, which will allow for the investigation of more detailed molecular interactions and for the study of the mechanism of enzymatic activity.

ACKNOWLEDGMENT

We thank Drs. Yasushi Oda, Haruki Nakamura, Shigenori Kanaya, Katsuo Katayanagi, and Kosuke Morikawa for their helpful discussion on the structure and function of RNase H.

APPENDIX

Table IV shows chemical shifts of ^{1}H, ^{13}C, and ^{15}N nuclei in *E. coli* RNase H at 27 °C in 0.1 M acetate buffer adjusted to pH 5.5. The ^{1}H chemical shifts are relative to internal TSP. The ^{13}C chemical shifts are relative to external TMS. The ^{15}N chemical shifts are relative to external liquid NH_3.

Table IV

	N′	H^N	C^α	H^α	C′	C^β	H^β
A24	126.0	9.52	49.2	5.89	173.7	21.3	1.53
A37	120.8	6.37	50.2	4.25	172.1	19.7	1.33
A51	117.0	7.72	53.3	3.31	175.5	19.3	1.69
A52	113.7	6.47	52.7	3.99	176.1	15.3	1.47
A55	119.4	6.85	52.7	3.34	175.6	17.2	1.16
A58	119.6	7.10	51.2	4.11	176.1	17.2	1.38
A93	123.6	9.10	53.1	4.07	175.8	16.0	1.46
A109	119.1	7.88	52.9	4.20	178.4	15.8	1.55
A110	121.0	7.67	52.7	4.30	178.1	16.5	1.60
A125	123.5	8.14	50.8	4.45	176.1	16.4	1.37
A137	122.7	8.35	53.5	3.62	177.3	16.6	1.41
A139	120.4	7.89	52.9	4.04	178.9	15.7	1.42
A140	121.8	7.88	52.7	3.98	177.7	15.3	1.20
A141	119.2	7.79	52.7	3.75	175.8	16.0	1.26

	N′	H^N	C^α	H^α	C′	C^β	H^β
C13	123.2	8.44	56.6	4.96	171.6	27.8	2.60
C63	125.3		57.0	5.12	171.6	29.3	2.66
C133	117.8	8.10	63.2	4.01	174.2	24.7	2.84/3.33

	N′	H^N	C^α	H^α	C′	C^β	H^β	C^γ
D10	120.2	9.06	52.7	5.16	171.2	43.0	2.68/2.74	175.5
D70	127.7	8.94	51.2	5.45	175.0	38.7	2.52/3.10	177.8
D94	114.0	8.00	51.2	4.64	172.7	37.5	2.64/2.80	178.4
D102	119.0	8.59	54.3	4.09	176.6	37.1	2.39/2.81	179.1
C108	118.4	8.76	56.6	4.56	176.1	41.7	3.04/3.22	176.4
D134	120.8	7.78	55.3	4.46	175.3	39.1	2.81	176.5
D148	125.6	10.04	50.4	4.88	175.5	36.8	2.30/3.40	177.6

	N′	H^N	C^α	H^α	C′	C^β	H^β	C^γ	H^γ	C^δ
E6	124.1	8.64	53.1	4.83	172.5	31.0	2.00	34.8	2.06/2.24	182.1
E32	122.7	8.76	53.1	5.43	173.9	31.1	1.86/1.96	34.8	2.00/2.23	180.4
E48	119.3	8.44	57.8	3.86	177.5			34.8	2.56/2.73	181.4
E57	118.4	8.75	56.6	3.94	175.3	29.4	1.88	35.6	2.23/2.66	182.1
E61	116.4	7.66	52.2	4.48	172.4	29.8	2.06	33.6	2.07	182.3
E64	122.6	8.75	53.7	5.02	172.7	28.5	1.92/2.04	34.5	2.14/2.27	180.8
E119	126.5	8.94	52.5	4.34	171.4	28.1	1.58/1.98	33.6	2.00/2.08	181.5
E129	117.8	9.37	59.0	3.63	176.8	25.3	0.72	34.8	1.48/1.77	181.2
E131	120.2	7.83	57.8	3.92	177.0	27.1	2.16	33.7	2.36/2.28	180.7
E135	118.9	7.83	57.8	3.92	178.0	27.1	2.16	33.7	2.50/2.30	180.9
E147	117.9	8.35	52.5	4.82	175.1	29.3	1.99	34.1	2.21/2.35	182.8
E154	125.2	8.26	54.5	4.34	173.4	28.1	1.94/2.06	34.1	2.30	182.1

	N′	H^N	C^α	H^α	C′	C^β	H^β	C^γ	C^δ	H^δ	C^ϵ	H^ϵ	C^ζ	H^ζ
F8	128.2	9.13	53.5	5.67	173.3	40.2	2.66/2.89	136.9	131.1	7.20				
F35	120.6	9.31	54.5	4.99	172.9	41.0	2.96/3.50	136.9	130.1	7.18	128.7	7.20	127.5	7.10

	N′	H^N	C^α	H^α	C′
G11	106.7	8.70	42.4	3.39/5.04	168.8
G15	107.6	7.82	42.8	3.83/4.11	169.3
G18	105.3	8.32	43.8	3.90/4.30	167.2
G20	108.4	8.96	43.8	3.76/5.07	168.9
G21	106.5	9.04	44.6	4.22/5.36	169.0
G23	106.2	8.99	43.4	3.90/5.17	169.1
G30	104.9	8.72	43.6	3.61/4.14	171.7
G38	106.2	8.58	42.2	3.49/5.36	170.8
G77	107.1	7.82	46.1	3.14/3.75	172.5
G89	108.7	7.78	45.3	3.93	172.7
G112	101.5	7.54	44.4	3.95/4.13	172.9
G123	111.3	8.46	43.4	3.91/4.07	171.4
G126	109.8	8.66	43.4	3.82	171.4
G150	106.7	8.02	43.0	3.73/4.21	172.0

	N′	H^N	C^α	H^α	C′	C^β	H^β	C^γ	$N^{\delta1}$	$C^{\epsilon1}$	$H^{\epsilon1}$	$C^{\delta2}$	$H^{\delta2}$	$N^{\epsilon2}$
H62	119.2	8.46	54.2	4.77	173.2	26.8	3.24	129.0	177.5	134.4	8.65	118.5	7.34	174.3
H83	118.4	7.93	56.9	4.13	175.5	26.2	3.08	130.0	198.1	135.4	8.43	177.8	7.12	175.3
H114	116.6	7.37	53.4	5.04	172.1	33.2	2.38/3.10	134.7	247.7	138.7	8.18	116.5	7.09	163.1
H124	116.5	8.57	54.2	4.64	172.4	26.5	3.24/3.38	129.9	182.3	134.8	8.63	117.3	7.25	174.3
H127	118.5	8.40	51.1	5.23	171.2	26.2	3.27/3.71	129.2	177.3	134.4	8.74	119.5	7.52	175.8

Table IV (Continued)

	N′	H^N	C^α	H^α	C′	C^β	H^β	$C^{\gamma 1}$	$H^{\gamma 1}$	$C^{\delta 1}$	$H^{\delta 1}$	$C^{\gamma 2}$	$H^{\gamma 2}$
I7	121.8	8.60	57.6	5.33	171.4	40.0	1.14	26.6	0.94/1.50	12.0	0.50	16.9	0.70
I25	120.7	9.04	58.4	4.88	171.8	41.6	1.52	25.8	0.98/1.76	12.4	0.77	14.8	0.84
I53	116.5	7.94	64.3	3.13	175.0	36.9	1.70	28.9	0.42/1.78	14.4	0.80	15.1	0.61
I66	127.4	8.25	58.0	4.75	172.7	36.9	1.60	25.8	0.94/1.44	11.7	0.77	15.5	0.66
I78	119.9	8.40	59.2	3.73	176.4	33.8	1.80	24.3	0.50/1.66	8.1	0.82	14.3	0.43
I82	117.9	8.48	64.2	3.49	174.1	35.5	1.52	28.2	1.55/1.24	12.5	1.26	14.9	0.88
I116	125.9	8.57	57.9	4.54	173.1	38.9	1.52	25.4	1.28/1.64	12.3	0.61	14.0	−0.32

	N′	H^N	C^α	H^α	C′	C^β	H^β	C^γ	H^γ	C^δ	H^δ	C^ϵ	H^ϵ	N^ζ
K3	123.8	8.73	55.1	4.31	173.2	31.2	1.84	23.2	1.32/1.46	27.1	1.43	39.5	2.64/2.74	31.3
K33	125.0	9.21	53.1	4.67	172.5	34.5	1.73	23.2	1.30	27.5	1.72	40.3	2.92	31.4
K60	121.8	8.59	53.9	4.38	173.8	30.2	1.82	22.4	1.47	26.3	1.66	40.3	3.02	
K86	119.0	8.12	58.2	2.70	177.7	30.1	1.34/1.66	24.0	1.22/1.08	27.9	1.80	39.5	3.05	
K87	119.0	7.36	56.6	4.09	175.5	29.8	1.88	22.8	1.50	27.1	1.66	39.5	2.96	
K91	116.7	6.82	52.0	5.05	174.5	35.1	1.67	23.2	1.22/1.44	27.1	1.58/1.46	40.0	3.00	
K95	112.5	8.06	55.8	3.67	173.1	27.0	2.02/2.16	23.6	1.36	27.1	1.69	39.9	3.01	
K96	119.8	7.62	51.6	4.72	171.5	30.2	1.66/1.82	23.2	1.30	27.1	1.66	40.3	2.96	
K99	127.9	8.29	55.5	4.05	175.7	29.7	1.80	22.8	1.44	27.1	1.77	39.9	3.05	
K117	129.8	8.81	52.7	4.48	171.8	32.0	1.64/1.76	23.2	1.30/1.38	27.4	1.66	40.3	2.94	31.3
K122	124.3	8.46	53.9	4.54	174.8	31.7	1.81/1.92	23.2	1.50	27.1	1.74	40.3	3.05	

	N′	H^N	C^α	H^α	C′	C^β	H^β	C^γ	H^γ	$C^{\delta 1}$	$H^{\delta 1}$	$C^{\delta 2}$	$H^{\delta 2}$
L2	125.1	8.71	52.7	4.55	174.8	41.0	1.62/1.71	24.7	1.64	22.8	0.83	21.2	0.86
L14	128.3	9.05	53.5	4.49	175.0	40.2	1.73	25.0	1.68	23.4	0.86	20.5	0.83
L26	129.2	9.21	52.1	5.29	173.1	44.1	1.60/1.92	27.1	1.64	23.4	0.94	23.8	0.94
L49	116.1	7.24	55.5	3.96	176.1	41.6	1.08/1.76	24.7	1.44	23.5	0.12	21.3	−0.29
L56	112.8	7.57	55.2	3.76	179.5	40.8	1.16/1.84	25.5	1.62	24.3	0.64	21.6	0.46
L59	118.4	7.15	52.4	4.26	175.0	40.0	1.42/1.98	23.9	1.82	23.4	0.30	21.2	0.74
L67	134.5	8.57	53.0	4.70	172.1	41.7	0.48/1.06	27.8	1.14	23.7	0.37	20.9	0.73
L103	118.6	7.28	53.5	4.16	177.1	40.7	1.08/1.60	24.3	1.68	24.6	0.75	19.2	0.58
L107	121.6	8.76	56.2	4.12	175.7	38.8	1.44/2.29	25.5	1.85	21.6	0.99	25.0	1.13
L111	117.4	8.68	55.5	4.10	177.6	39.5	1.76/2.28	24.7	2.27	23.9	1.22	22.5	1.08
L136	120.1	8.30	55.5	4.02	177.3	41.6	1.48/2.06	24.7	1.88	23.8	0.88	20.7	0.88
L146	123.4	8.08	51.9	4.76	173.8	43.4	1.12/0.80	23.9	1.55	24.2	0.58	20.5	0.83

	N′	H^N	C^α	H^α	C′	C^β	H^β	C^γ	H^γ	C^ϵ	H^ϵ
M1	37.1		53.1	4.17	170.2	30.9	2.20	29.0	2.64	14.5	2.09
M47	118.2	7.71	55.5	4.44	176.4					17.3	1.52
M50	118.7	8.69	55.5	3.93	174.5	29.4	1.84	31.0	2.32/2.10	14.7	1.70
M142	111.0	7.11	53.9	4.29	174.4	31.0	2.20/2.10	30.6	2.63/2.80	14.8	2.14

	N′	H^N	C^α	H^α	C′	C^β	H^β	C^γ	$N^{\delta 2}$	$H^{\delta 2}$
N16	116.2	8.24	49.2	5.06	170.2	37.5	2.62/2.97	176.1	112.1	7.68/6.89
N44	120.6	9.19	56.0	3.92	175.1	36.8	2.78/2.86	173.5	113.2	7.66/6.90
N45	116.3	8.56	53.9	4.03	174.6	34.8	1.76/2.04	173.1	109.7	7.02/6.83
N84	117.7	7.44	53.5	4.38	175.7	36.3	2.68	173.8	113.0	7.54/7.02
N100	115.8	9.45	53.1	4.28	174.0	34.8	3.46/2.68	176.0	113.6	7.52
N130	117.2	7.66	56.6	4.45	175.3	36.7	2.80/3.14	174.3	108.2	8.39/7.05
N143	117.0	7.42	49.4	5.04	168.6	38.0	2.47/2.73	176.3	113.2	7.60/6.79

	N′	C^α	H^α	C′	C^β	H^β	C^γ	H^γ	C^δ	H^δ
P17	137.2	61.3	4.92	174.5	34.8	1.76/2.00	22.4	1.82/2.04	47.9	3.64/3.54
P19	137.2	61.3	4.92	174.8	30.1	2.34	26.0	2.23	47.4	3.64
P97	133.5	60.9	4.61	175.1	30.1	2.35/1.80	26.3	2.00/2.10	48.3	3.64/3.86
P128	138.4	63.6	4.39	177.4	29.3	1.84/2.34	25.5	2.08	48.5	3.86/3.73
P144	136.1	62.1	4.10	175.2	30.2	1.56/1.99	25.5	1.98/2.10	47.4	3.50

	N′	H^N	C^α	H^α	C′	C^β	H^β	C^γ	H^γ	C^δ	$N^{\epsilon 2}$	$H^{\epsilon 2}$
Q4	122.8	8.31	53.3	5.13	173.5	28.5	2.08	32.5	2.28	178.6	113.2	7.72/6.88
Q72	132.8	9.37	56.2	3.98	175.5	26.5	2.17	32.0	2.52	178.1	113.2	7.53/6.94
Q76	120.6	8.22	57.0	3.15	175.7	25.5	0.56/1.36	32.5	1.61/1.94	177.8	110.0	6.90/6.78
Q80	117.3	7.53	55.1	4.47	175.2	29.3	1.56/1.32	31.3	2.00	178.0	110.7	7.02/6.73
Q105	115.8	8.42	57.4	3.66	177.3	25.9	1.60/1.74	31.7	1.48/0.90	177.3	108.4	6.54/5.08
Q113	117.2	7.52	53.5	4.27	173.2	26.6	1.77/1.64	31.6	2.27	178.2	112.4	7.39/6.77
Q115	120.9	8.48	52.7	4.74	172.7	27.8	2.05	31.7	2.36	178.4	112.2	7.62/6.84
Q152	126.0	7.60	52.3	4.15	172.2	28.1	1.77/1.94	31.3	2.21	178.7	112.2	7.45/6.81

Table IV (Continued)

	N′	H^N	C^α	H^α	C′	C^β	H^β	C^γ	H^γ	C^δ	H^δ	N^ϵ	H^ϵ	C^ζ	N^η	H^η
R27	127.1	9.98	53.1	5.47	172.2	31.6	2.20/1.64	25.1	1.54/1.73	41.8	3.30	82.7	7.36	158.0		
R29	126.7	9.37	55.1	3.78	174.4	26.2	1.33/1.84	25.2	0.96/1.23	41.8	3.02	84.8	7.07	157.5		
R31	121.0	7.95	52.9	4.69	173.2	30.1	1.88	25.1	1.66	41.1	3.24	84.7	7.23	157.6		
R41	119.9	7.77	55.1	3.88	170.6	29.3	1.80/1.60	25.9	1.18/1.34	41.4	3.19	83.9	7.32	157.6		
R46	116.5	7.38	59.0	3.58	176.4					40.3	2.80/3.72	81.7	10.14	158.3	72.4	8.19/8.41
R75	117.7	7.08	57.4	2.52	177.7	27.4	0.72/1.22	23.9	0.40/−0.70	41.1	2.33/2.48	83.7	6.48	157.2		
R88	116.3	7.24	53.1	4.48	174.6	28.6	2.12/1.82	25.5	1.69	41.4	3.10	85.2	7.28	157.5		
R106	121	7.02	57.4	4.18	177.4	29.3	1.92	24.4	1.56/1.92	42.6	2.81/3.30	83.9	8.54	157.9		
R132	119.8	8.02	57.4	4.09	177.4	28.6	1.88	24.7	1.77	41.8	3.02/3.27	83.4	7.18	157.9		
R138	116.5	8.24	57.6	3.80	177.0	28.0	1.79	27.1	1.58/1.78	41.1	3.16	85.8	7.52	157.5		

	N′	H^N	C^α	H^α	C′	C^β	H^β
S12	113.5	8.80	55.8	4.78	171.7	63.5	3.38/3.72
S36	113.9	8.40	56.2	4.58	170.3	63.5	3.90/3.96
S68	120.8	8.72	54.5	5.73	172.5	62.8	3.79/3.68
S71	115.5	8.31	56.8	4.52	174.5	61.2	4.05/4.15

	N′	H^N	C^α	H^α	C′	C^β	H^β	$C^{\gamma 2}$	$H^{\gamma 2}$
T9	109.5	8.05	58.8	5.61	173.2	69.4	4.36	21.0	0.96
T34	114.5	8.14	58.2	5.32	171.4	69.0	4.06	19.9	1.16
T40	113.5	8.81	63.6	3.73	173.1	67.0	4.24	20.2	1.18
T42	125.0	8.85	58.0	4.08	169.3	65.4	4.16	16.0	1.26
T43	106.5	8.53	57.0	5.28	173.4	70.5	4.56	20.7	1.12
T69	119.7	8.50	58.6	5.11	170.6	67.0	4.67	16.8	1.54
T79	107.4	7.80	62.1	4.11	173.9	68.4	4.04	19.3	1.18
T92	109.6	8.90	59.0	4.38	175.0	69.0	4.66	20.5	1.11
T145	108.4	7.49	59.3	4.56	172.1	69.0	4.33	19.7	1.14
T149	116.6	7.88	62.5	4.14	173.8	66.7	4.38	19.9	1.34

	N′	H^N	C^α	H^α	C′	C^β	H^β	C^γ	$C^{\delta 1}$	$H^{\delta 1}$	$N^{\epsilon 1}$	$H^{\epsilon 1}$
W81	118.2	7.10	55.8	4.28	175.9	26.5	1.74/0.67	108.7	122.4	6.66	128.1	10.05
W85	120.3	8.20	55.8	4.38	177.8	27.8	2.28/2.82	109.6	121.0	6.81	127.1	9.69
W90	112.8	8.56	56.2	3.42	172.2	22.0	3.26/3.46	110.4	125.2	7.18	130.1	10.60
W104	121.0	8.55	59.3	4.56	177.1	28.5	2.90/3.61	109.0	126.6	7.08	127.4	9.68
W118	125.9	8.26	54.1	4.46	174.0	29.0	2.30/1.38	110.4	125.9	7.18	128.4	10.12
W120	125.8	7.93	52.0	5.62	175.2	27.5	3.20/3.38	109.0	126.2	7.27	127.6	9.96

$C^{\delta 2}$	$C^{\epsilon 2}$	$C^{\zeta 2}$	$H^{\zeta 2}$	$C^{\eta 2}$	$H^{\eta 2}$	$C^{\epsilon 3}$	$H^{\epsilon 3}$	$C^{\zeta 3}$	$H^{\zeta 3}$
	136.7	112.8	7.40	122.7	7.31			120.5	6.98
127.4	136.9	112.4	6.69	122.7	6.46	117.1	6.94	118.6	4.92
126.8	137.1	112.8	7.56	121.8	7.15	117.4	7.10	119.7	7.04
	137.5	113.1	6.67	122.7	7.27	119.1	7.80	119.0	6.95
	136.7	112.0	7.39	119.9	6.84				
126.8	137.5	111.8	6.57	123.1	5.78	119.7	7.78	118.7	6.63

	N′	H^N	C^α	H^α	C′	C^β	H^β	$C^{\gamma 1}$	$H^{\gamma 1}$	$C^{\gamma 2}$	$H^{\gamma 2}$
V5	121.8	8.79	58.4	4.82	172.7	32.5	1.92	19.6	0.84	19.4	0.75
V54	116.5	8.25	64.1	3.30	176.1	29.3	1.46	18.0	0.66	19.7	0.66
V65	125.6	8.82	58.0	4.70	173.4	33.8	1.59	19.6	0.41	19.4	0.36
V74	117.4	8.06	64.6	3.60	174.7	30.1	1.98	20.0	1.01	20.9	1.09
V98	120.7	7.57	59.8	3.44	174.2	30.5	1.27	17.1	−0.30	18.0	−0.05
V101	119.0	7.65	63.6	3.60	171.5	28.2	2.50	16.6	0.94	20.4	0.83
V121	123.6	8.03	59.4	4.20	173.3	31.5	1.62	19.5	0.68	18.3	0.77
V153	120.6	7.86	60.5	3.84	173.9	30.1	1.99	19.0	0.92	18.7	0.95
V155	125.4	7.73	61.5	4.04	178.9	31.2	2.08	19.5	0.90	18.1	0.88

	N′	H^N	C^α	H^α	C′	C^β	H^β	C^γ	C^δ	H^δ	C^ϵ	H^ϵ	C^ζ
Y22	113.3	7.87	53.5	5.74	171.7	41.0	3.16/3.49	127.1	131.2	7.02	115.5	6.83	156.1
Y28	125.2	8.59	54.7	5.06	172.5	37.9	3.04	127.6	131.8	7.26	116.1	6.86	155.5
Y39	122.8	9.69	53.9	5.47	174.7	40.2	2.68	127.8	131.5	6.97	115.5	6.82	156.2
Y73	123.6	8.72	59.3	4.48	175.3	37.9	2.86/3.38	129.4	132.0	7.31	117.3	6.98	154.4
Y151	121.4	7.27	56.8	4.24	172.5	35.9	3.05	127.4	130.7	7.00	115.9	6.60	155.2

REFERENCES

Ando, I., Saito, H., Tabeta, R., Shoji, A., & Ozaki, T. (1984) *Macromolecules 17*, 457–461.

Bax, A., Clore, M., Driscoll, P. C., Gronenborn, A. M., Ikura, M., & Kay, L. E. (1990a) *J. Magn. Reson. 87*, 620–627.

Bax, A., Clore, M., & Gronenborn, A. M. (1990b) *J. Magn. Reson. 88*, 425–431.

Blomberg, F., & Rüterjans, H. (1983) *Biol. Magn. Reson. 5*, 21–73.

Clore, G. M., Bax, A., Driscoll, P. C., Wingfield, P. T., & Gronenborn, A. M. (1990) *Biochemistry 29*, 8172–8184.

Crouch, R. J., & Dirksen, M.-L. (1982) in *Nuclease* (Linn, S. M., & Roberts, R. J., Eds.) pp 211–241, Cold Spring Harbor Laboratory, Cold Spring Harbor, NY.

Ernst, R., Bodenhausen, G., & Wokaun, A. (1987) *Principles of Nuclear Magnetic Resonance in One and Two Dimensions*, Clarendon Press, Oxford.

Fesik, S. W., & Zuiderweg, E. R. P. (1988) *J. Magn. Reson. 78*, 588–593.

Glushka, J., Lee, M., Coffin, S., & Cowburn, D. (1989a) *J. Am. Chem. Soc. 111*, 7716–7722.

Glushka, J., Lee, M., Coffin, S., & Cowburn, D. (1989b) *J. Am. Chem. Soc. 111*, 2843.

Ikura, M., Kay, L. E., & Bax, A. (1990) *Biochemistry 29*, 4659–4667.
Ikura, M., Spera, S., Barbato, G., Kay, L. E., Krinks, M., & Bax, A. (1991) *Biochemistry 30*, 9216–9228.
Itaya, M. (1990) *Proc. Natl. Acad. Sci. U.S.A. 87*, 8587–8591.
Kanaya, S., Kohara, A., Miura, Y., Sekiguchi, A., Iwai, S., Inoue, H., Ohtsuka, E., & Ikehara, M. (1990) *J. Biol. Chem. 265*, 4615–4621.
Kanaya, S., Oobatake, M., Nakamura, H., & Ikehara, M. (1992) *J. Biotechnol.* (submitted).
Katayanagi, K., Miyagawa, M., Matsushima, M., Ishikawa, S., Kanaya, S., Ikehara, M., Matsuzaki, T., & Morikawa, K. (1990) *Nature 347*, 306–309.
Katayanagi, K., Miyagawa, M., Matsushima, M., Ishikawa, M., Kanaya, S., Nakamura, H., Ikehara, M., Matsuzaki, T., & Morikawa, K. (1992) *J. Mol. Biol. 223*, 1029–1052.
Kay, L. E., Ikura, M., Tshudin, R., & Bax, A. (1990a) *J. Magn. Reson. 89*, 496–514.
Kay, L. E., Ikura, M., & Bax, A. (1990b) *J. Am. Chem. Soc. 112*, 888–889.
Kawano, K., & Kyogoku, Y. (1975) *Chem. Lett.*, 1305–1308.
Marion, D., Kay, L. E., Sparks, S. W., Torchia, D. A., & Bax, A. (1989a) *J. Am. Chem. Soc. 111*, 1515–1517.
Marion, D., Driscoll, P. C., Kay, L. E., Wingfield, P. T., Bax, A., Gronenborn, A. M., & Clore, G. M. (1989b) *Biochemistry 28*, 6150–6156.
Martin, G. J., Martin, M. L., & Gouesnard, J.-P. (1981) *^{15}N-NMR Spectroscopy*, Springer-Verlag, New York.
Nagayama, K., Yamazaki, T., Yoshida, M., Kanaya, S., & Nakamura, H. (1990) *J. Biochem. (Tokyo) 108*, 149–152.
Nakamura, H., Oda, Y., Iwai, S., Inoue, H., Ohtsuka, E., Kanaya, S., Kimura, S., Katsuda, C., Katayanagi, K., Morikawa, K., Miyashiro, H., & Ikehara, M. (1991) *Proc. Natl. Acad. Sci. U.S.A. 88*, 11525–11539.
Oda, Y., Nakamura, H., Kanaya, S., & Ikehara, M. (1991) *J. Biomol. NMR 1*, 247–255.
Oda, Y., Nakamura, H., Yamazaki, T., Nagayama, K., Yoshida, M., Kanaya, S., & Ikehara, M. (1992) *J. Biomol. NMR 2*, 137–147.
Oh, B.-H., & Markley, J. L. (1990) *Biochemistry 29*, 3993–4004.
Oh, B.-H., Westler, M. W., Darba, P., & Markley, J. L. (1988) *Science 240*, 908–911.
Oh, B.-H., Mooberry, E. S., & Markley, J. L. (1990) *Biochemistry 29*, 4004–4011.
Oschkinat, H., Griesinger, C., Kraulis, P. J., Sørensen, O. W., Ernst, R. R., Gronenborn, A. M., & Clore, G. M. (1988) *Nature 332*, 374–376.
Pelton, J. G., Torchia, D. A., Meadow, N. D., Wong, C.-Y., & Roseman, S. (1991) *Biochemistry 30*, 10043–10057.
Powers, R., Gronenborn, A. M., Clore, G. M., & Bax, A. (1991a) *J. Magn. Reson. 94*, 209–213.
Powers, R., Clore, G. M., Bax, A., Garrett, D. S., Stahl, S. J., Wingfield, P. T., & Gronenborn, A. M. (1991b) *J. Mol. Biol. 221*, 1081–1090.
Richarz, R., & Wüthrich, K. (1978) *Biopolymers 17*, 2133–2141.
Senn, H., Werner, B., Messerle, B. A., Weber, C., Traber, R., & Wüthrich, K. (1989) *FEBS Lett. 249*, 113–118.
Spera, S., & Bax, A. (1991) *J. Am. Chem. Soc. 113*, 5490–5492.
Vuister, G. W., Boelens, R., & Kaptein, R. (1988) *J. Magn. Reson. 80*, 176–185.
Wishart, D. S., Sykes, B. D., & Richards, F. M. (1991) *J. Mol. Biol. 222*, 311–333.
Wishart, D. S., Sykes, B. D., & Richards, F. M. (1992) *Biochemistry 21*, 1647–1651.
Wüthrich, K. (1986) *NMR of Proteins and Nucleic Acids*, John Wiley & Sons, New York.
Yamazaki, T., Yoshida, M., Kanaya, S., Nakamura, H., & Nagayama, K. (1991) *Biochemistry 30*, 6036–6047.
Yang, W., Hendrickson, W. A., Crouch, R. J., & Satow, Y. (1991) *Science 249*, 1398–1405.
Zuiderweg, E. R. P., & Fesik, S. W. (1989) *Biochemistry 28*, 2387–2391.